Geophys. J. Int. (2008) **174,** 1153–1173 doi: 10.1111/j.1365-246X.2008.03860.x

Seamount volcanism along the Gakkel Ridge, Arctic Ocean

James R. Cochran

Lamont Doherty Earth Observatory of Columbia University, Palisades, New York, USA. E-mail: jrc@ldeo.columbia.edu

Accepted 2008 May 21. Received 2008 May 21; in original form 2007 June 8

SUMMARY

The Gakkel Ridge in the Arctic Ocean is the slowest spreading portion of the global mid-ocean ridge system. Total spreading rates vary from 12.8 mm yr^{-1} near Greenland to 6.5 mm yr^{-1} at the Siberian margin. Melting models predict a dramatic decrease in magma production and resulting crustal thickness at these low spreading rates. At slow spreading ridges, small volcanic seamounts are a dominant morphologic feature of the rift valley floor and an important mechanism in building the oceanic crust. This study quantitatively investigates the extent, nature and distribution of seamount volcanism at the ultraslow Gakkel Ridge, the manner in which it varies along the ridge axis and the relationship of the volcanoes to the larger scale rift morphology. A numerical algorithm is used to identify and characterize isolated volcanic edifices by searching gridded swath-bathymetry data for closed concentric contours protruding above the surrounding seafloor. A maximum likelihood model is used to estimate the total number of seamounts and the characteristic height within different seamount populations. Both the number and size of constructional volcanic features is greatly reduced at the Gakkel Ridge compared with the Mid-Atlantic Ridge (MAR). The density of seamounts (number/area) on the rift valley floor of the Western Volcanic Zone (WVZ) is ∼55% that of the MAR. The observed volcanoes are also much smaller, so, the amount of erupted material is greatly reduced compared with the MAR. However, the WVZ is still able to maintain a MAR-like morphology with axial volcanic ridges, volcanoes scattered on the valley floor and rift valley walls consisting of high-angle faults. Seamount density at the Eastern Volcanic Zone (EVZ) is ∼45% that of the WVZ (∼25% that of the MAR). Seamounts are clustered at the widely spaced magmatic centres characteristic of the EVZ, although some seamounts are found between magmatic centres. These seamounts tend to be located at the edge of the rift valley or on the valley walls rather than on the valley floor. Seamounts in the Sparsely Magmatic Zone (SMZ) are located almost entirely at the 19°E magmatic centre with none observed within a 185 km-long portion of the rift valley floor. The EVZ and SMZ appear to display a mode of crustal accretion, characterized by extreme focusing of melt to the magmatic centres. Magmas erupted between the magmatic centres appear to have ascended along faults. This is very different from what is observed at the WVZ (or the MAR), and there is a threshold transition between the two modes of crustal accretion. At the Gakkel Ridge, the location of the transition appears to be localized by a boundary in mantle composition.

Key words: Mid-ocean ridge processes; Effusive volcanism; Eruption mechanisms and flow emplacement; Arctic region.

INTRODUCTION

The Gakkel Ridge, the spreading centre in the Eurasian Basin of the Arctic Ocean (Fig. 1), is the slowest spreading section of the global mid-ocean ridge system. Total spreading rates vary from 12.8 mm yr^{-1} at 83°N, 6°W near the intersection of the Gakkel Ridge and the Lena Trough to 6.5 mm yr^{-1} at 78.5°N, 128°E near the Siberian continental margin (Karasik 1968; Vogt *et al.* 1979; DeMets *et al.* 1994; Brozena *et al.* 2003). For comparison, spreading rates along the Southwest Indian Ridge (SWIR), the other 'ultra-slow' spreading ridge, vary between about 16 and 12 mm yr^{-1} (Patriat 1987; Patriat & Segoufin 1988; DeMets *et al.* 1994; Chu & Gordon 1999). Despite its extremely low spreading rate, a well-defined, localized ridge axis, identifiable through bathymetry, seismic reflection and potential field data (Vogt *et al.* 1979; Sekretov 1998, 2002; Cochran *et al.* 2003) and flanked by lineated ridge-parallel magnetic anomalies interpreted as a seafloor spreading anomaly sequence (e.g. Karasik 1968; Vogt *et al.* 1979; Glebovsky *et al.* 2000, 2006; Brozena *et al.* 2003), is present along nearly the entire length of the Gakkel Ridge. Organized seafloor spreading appears to be occurring even at the very slow spreading rates found at the Gakkel Ridge.

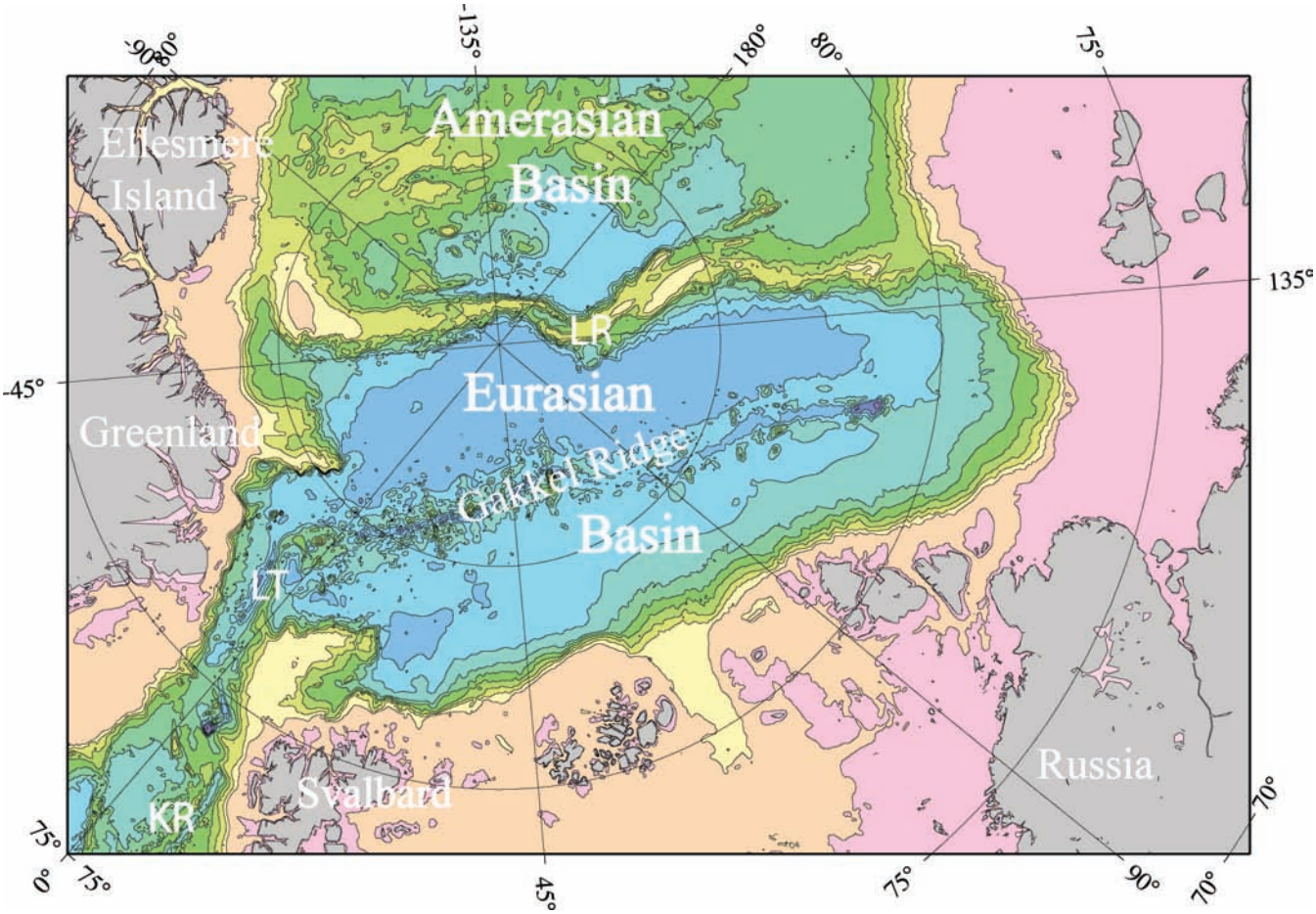

Figure 1. Bathymetric map showing the location of the Gakkel Ridge within the Eurasian Basin of the Arctic Ocean. Other bathymetric features identified include the Lena Trough (LR), Lomonosov Ridge (LR) and Knipovich Ridge (KR).

Melting models based on decompression melting of mantle, which is upwelling in response to corner flow driven by plate separation, predict that melt production, and thus crustal thickness, should decrease significantly at total spreading rates below ∼15–20 mm yr^{-1} (e.g. Reid & Jackson 1981; Bown & White 1994). The limited amount of seismic refraction and other geophysical data available from ultra-slow spreading ridges supports this prediction. Klingelhofer *et al.* (2000) obtained a mean crustal thickness of ∼4 km from an ocean bottom seismometer (OBS) experiment near 72°N on Mohns Ridge, where the spreading rate is 15.8 mm yr^{-1} (14 mm yr^{-1} opening perpendicular to the axis). Also Minshull *et al.* (2006) determined an average crustal thickness of 4.2 km from a set of seismic refraction experiments at the SWIR axis near 66°E, where the observed spreading rate is in the range of 13.5–15 mm yr^{-1} (Cannat *et al.* 2003). In both cases, a very thin layer 3 is the main difference from 'normal' 6–7 km-thick oceanic crust (e.g. White *et al.* 1992).

Coakley & Cochran (1998) concluded on the basis of gravity data that crust at the axis of the Gakkel Ridge has to be less, and perhaps much less, than 4 km thick. Jokat *et al.* (2003) and Jokat & Schmidt-Aursch (2007) reported on 12 seismic refraction experiments in the Gakkel rift valley between 5°W and 67°E, carried out using receivers placed on the ice. Spreading rates in this portion of the Gakkel Ridge are between 12.7 and 10.5 mm yr^{-1}. They consistently found a thin crust (1.2–4.9 km thick), characterized by relatively low seismic velocities, generally < 6.0 km s^{-1}. This low velocity crust rests directly on a layer with compressional velocities of 7.4–7.8 km s^{-1}, interpreted as mantle. The low mantle velocities probably reflect serpentinization. Seismic velocities typical of oceanic layer 3 were not found (Jokat & Schmidt-Aursch 2007). It thus appears that the crust at the Gakkel Ridge may consist largely of basalts erupted onto peridotite. This is supported by the observation that gabbro was only rarely recovered during an extensive dredging programme in the Gakkel rift valley (Michael *et al.* 2003).

The greatly decreased melt production at the Gakkel Ridge can be expected to affect not only the crustal thickness and structure but also the style of volcanic activity at the ridge axis. In this study, we use multibeam bathymetric data to quantitatively investigate the form and distribution of volcanic edifices along the Gakkel Ridge and their relationship to the morphology of the ridge axis. A numerical algorithm (Behn *et al.* 2004) is used to identify isolated volcanic features and determine the location, height, volume and ellipticity of each. A maximum likelihood model (Smith & Jordan 1988) is used to characterize the population in a given area by determining the characteristic height and density (seamounts per 1000 km^2) of the seamount population within a given region.

BATHYMETRY DATA FROM THE GAKKEL RIDGE

The Gakkel Ridge has now been surveyed by two major expeditions using very different platforms and instrumentation. The SCience

ICe EXercises (SCICEX) programme utilized U.S. Navy nuclear submarines for a series of unclassified scientific research cruises to the Arctic Ocean between 1993 and 1999. In particular, 'USS Hawkbill' carried out a systematic survey of the Gakkel Ridge axis utilizing the SCAMP instrument package during the 1998 and 1999 cruises. These cruises obtained nearly complete bathymetry, sidescan and gravity coverage to 50 km from the ridge axis, for 600 km along the Gakkel Ridge, from 8°E to 73°E, with coverage of the axis to 96°E (Edwards *et al.* 2001; Cochran *et al.* 2003). The SCAMP bathymetric system (Chayes *et al.* 1996, 1997, 1999) is an interferometric instrument that produces extremely high resolution sidescan but only moderate resolution bathymetry. In addition, due to short period navigational noise, the data had to be low-pass filtered. As a result, features wider than a few km across are well imaged, but the small seamounts, which are the object of this study, have basically been removed from the data.

The Arctic Mid-Ocean Ridge Expedition (AMORE) programme utilized two icebreakers ('USCGC Healy' and 'PFS Polarstern') to carry out a swath-mapping, rock sampling and seismic refraction programme from 7°W to 86°E in 2001 (Edmonds *et al.* 2003; Jokat *et al.* 2003; Michael *et al.* 2003). Mapping was carried out with a Hydrosweep DS2 system on 'Polarstern' and a SeaBeam 2112 system on 'Healy'. Thiede (2002) estimated an absolute accuracy of about 0.5% of the water depth for both systems. The data are gridded into 50 m × 50 m cells, which is slightly less than the beam footprint. Thus, features wider than a few hundred metres can be resolved. These bathymetry data are of much higher resolution than the SCICEX data, but since AMORE was largely a rock-sampling programme, it did not carry out a systematic bathymetric survey and data are limited to the rift valley floor and portions of the walls, only rarely extending out of the rift valley.

The two data sets complement each other. The AMORE data provide high-resolution bathymetric data from the rift valley floor and portions of the walls (Figs 2, 3a and 4a). It serves as the database for our effort to identify and characterize volcanic edifices. The SCICEX data have much lower resolution, but systematically maps a broad region extending out of the rift valley onto the ridge flanks (Figs 3b and 4b). We utilize it to establish the tectonic context of the detailed AMORE data and to examine the relationship between

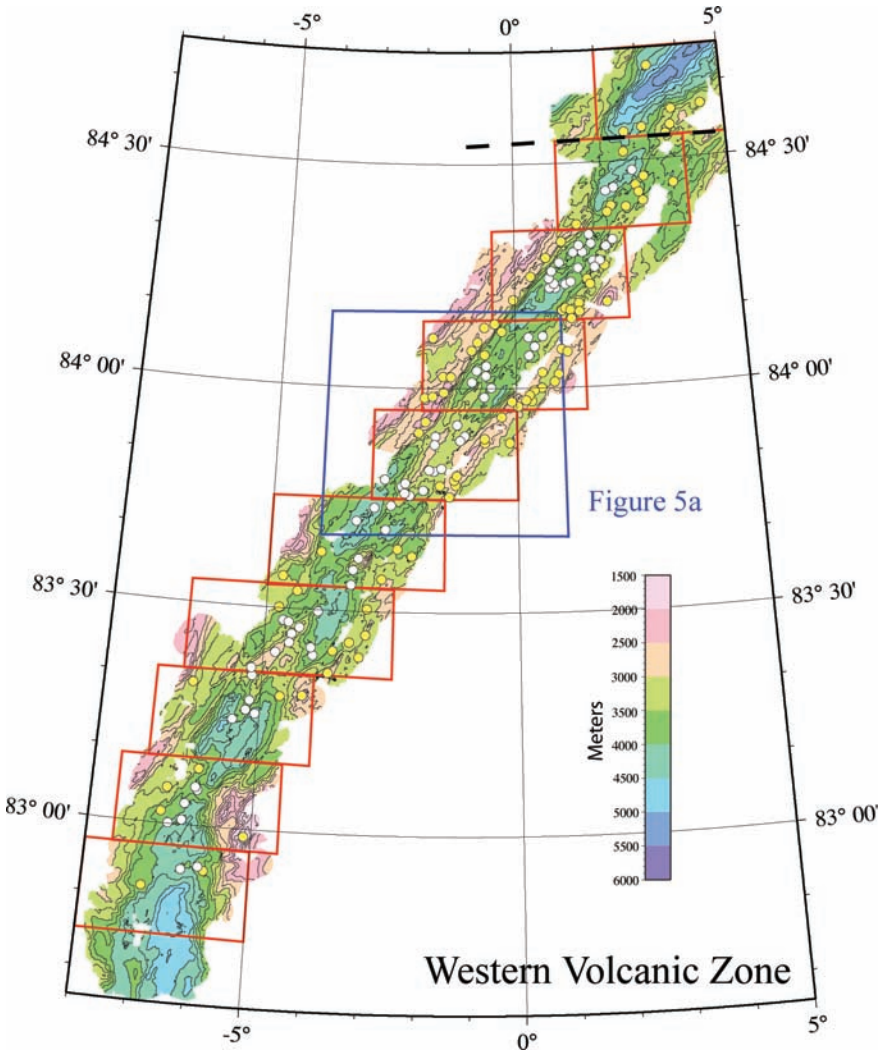

Figure 2. Bathymetry map of the Western Volcanic Zone (WVZ) based on AMORE data (Michael *et al.* 2003). Red boxes outline areas searched for seamounts. White dots show the location of seamounts with height >50 m, identified on the rift valley floor and yellow dots show the location of seamounts on the valley walls and flanks. Dashed black line shows the boundary between the WVZ and SMZ. Blue box outlines the region shown in Fig. 5a. Map is contoured at 250 m intervals.

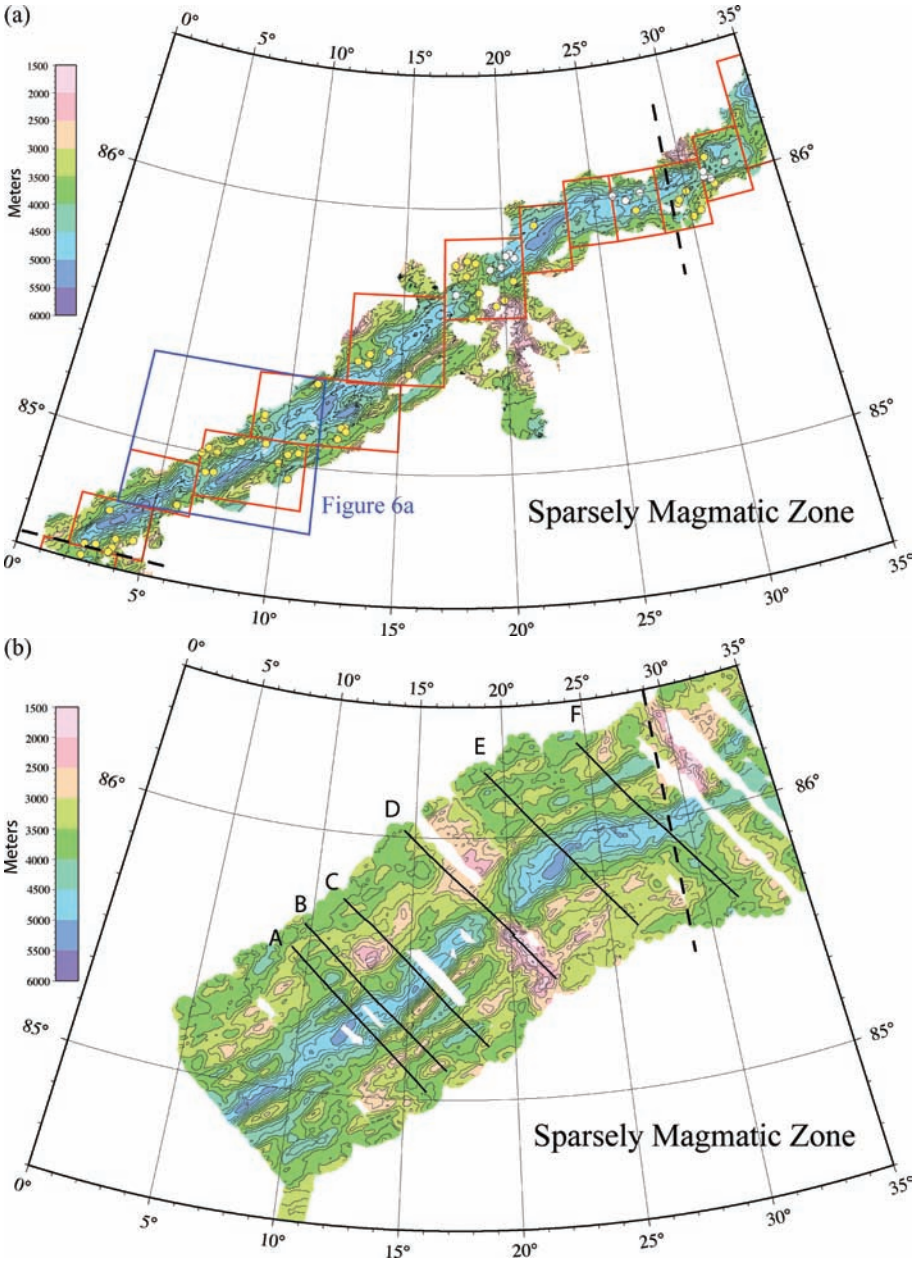

Figure 3. (a) Bathymetry map of the Sparsely Magmatic Zone (SMZ) based on AMORE data (Michael *et al.* 2003). Red boxes outline areas searched for seamounts. White dots show the location of seamounts identified with height >50 m on the rift valley floor and yellow dots show the location of seamounts on the valley walls and flanks. Dashed black lines show along-axis boundaries of the SMZ. Blue box outlines the region shown in Fig. 6a. Map is contoured at 250 m intervals. (b) Bathymetry map of the Sparsely Magmatic Zone (SMZ) based on SCICEX data (Cochran *et al.* 2003). Solid black lines show submarine tracks for profiles shown in Fig. 8. Dashed black line shows boundary between the SMZ and EVZ. Map is contoured at 250 m intervals.

the nature of volcanism in the rift valley and the structure of the rift valley and rift mountains.

GAKKEL RIDGE AXIAL BATHYMETRY

Michael *et al.* (2003) divided the Gakkel Ridge into three sections on the basis of bathymetry and rock recovery:

Western Volcanic Zone

The 'Western Volcanic Zone' (WVZ) extends about 220 km from the western end of the ridge near 83°N, 7°W to 84°30′N, 3°E (Fig. 2). This region is characterized by a relatively shallow (∼4200 m) rift valley, abundant recovery of basalt and numerous volcanic landforms (Michael *et al.* 2003). A series of bathymetric highs are located on the rift valley floor (Fig. 2). The two most prominent, centred near 83°24′N, 4°45′W and 83°52′N, 1°45′W, are elongate volcanic ridges extending for ∼40–50 km along the axis (Figs 2 and 5a). Two other bathymetric highs, near 83°05′N, 6°W and 83°37′N, 3°15′W are less elongate and extend for 15–30 km along-axis. A broader, less well-defined high is located in the north between about 84°12′N and 84°25′N. There is no axial volcanic ridge there, but nearly circular volcanic cones, a few kilometres across and up to 100–150 m high, are prominent features of the rift valley floor in this area.

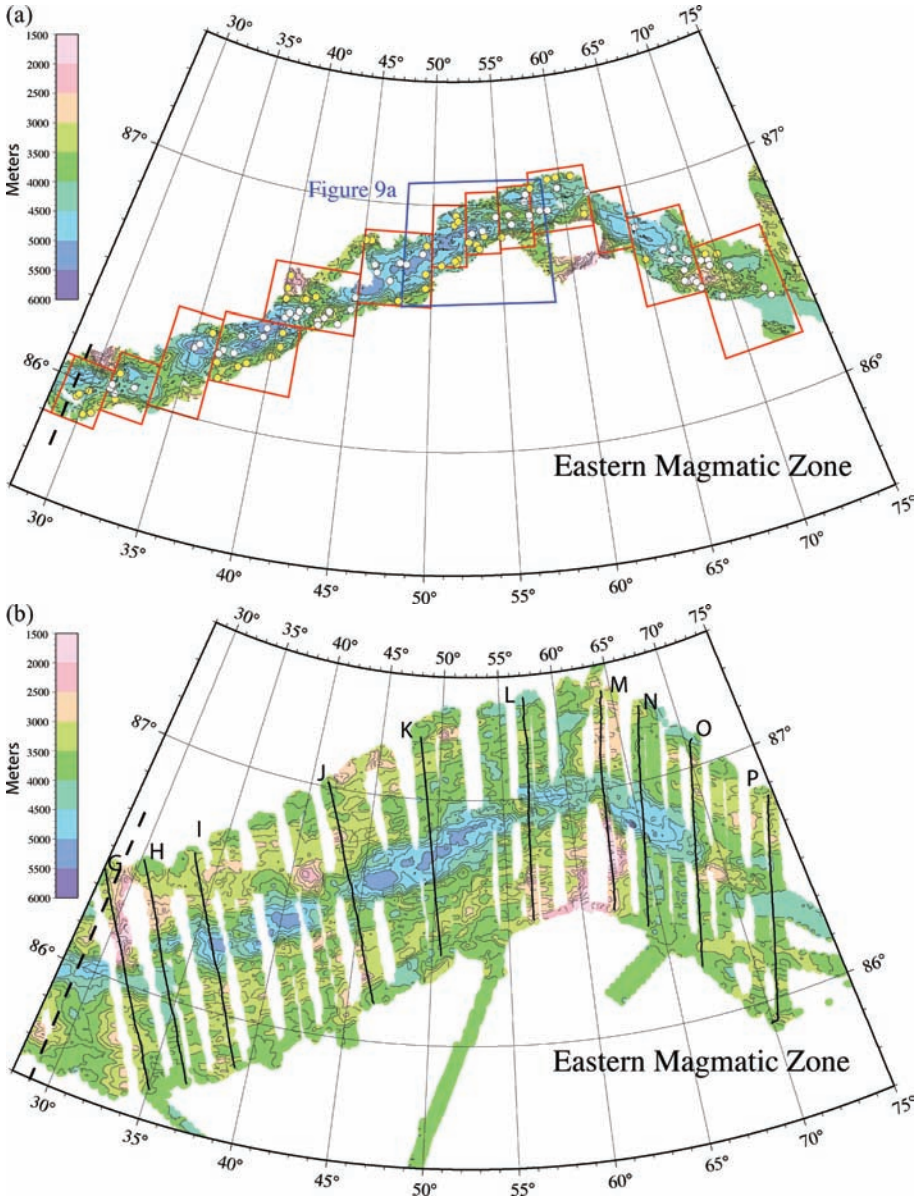

Figure 4. (a) Bathymetry map of the Eastern Volcanic Zone (EVZ) based on AMORE data (Michael *et al.* 2003). Red boxes outline areas searched for seamounts. White dots show the location of seamounts identified with height >50 m on the rift valley floor and yellow dots show the location of seamounts on the valley walls and flanks. Dashed black line shows the boundary between the EVZ and SMZ. Blue box outlines the region shown in Fig. 9a. Map is contoured at 250 m intervals. (b) Bathymetry map of the Eastern Volcanic Zone (EVZ) based on SCICEX data (Cochran *et al.* 2003). Solid black lines show submarine tracks for profiles shown in Fig. 8. Dashed black line shows boundary between the EVZ and SMZ. Map is contoured at 250 m intervals.

The rift valley narrows slightly at all of the bathymetric highs and the rift valley floor shallows by 500–1000 m across its entire width in a manner reminiscent of the intrasegment bathymetric highs along the Mid-Atlantic Ridge (MAR; e.g., Sempere *et al.* 1990, 1993; Detrick *et al.* 1995). Although these highs display the magmatic segmentation of the ridge, they are not separated by observable tectonic ridge axis discontinuities, suggesting that the segmentation is controlled by magmatic processes in the mantle rather than imposed by lithospheric tectonics (Michael *et al.* 2003).

The rift valley walls consist of sets of inward facing faults (Figs 5a and b) that form a pattern of scarps and terraces similar to those observed at the MAR (e.g. Needham & Francheteau 1974; Macdonald 1986). The size of individual scarps tends to become larger to the northeast of 83°55′N, giving the walls a steeper appearance. This is particular true on the northwestern wall, where scarp heights occasionally reach 1000 m (e.g. 83°59′N-84°03′N, Figs 5a and b).

Sparsely Magmatic Zone

The 'Sparsely Magmatic Zone' (SMZ) extends for about 275 km from near 84°38′N, 3°E to 86°N, 29°E (Figs 3a and b). The SMZ is separated from the WVZ by a 10 km left-stepping non-transform discontinuity. The eastern end of the SMZ is marked by an oblique spreading axis extending nearly east–west along 86°N for 25–30 km from 25°E to 29°E (Figs 3a and b).

The rift valley floor deepens rapidly east of the 3°E non-transform offset, reaching 5400 m within 5 km of the offset. The valley floor

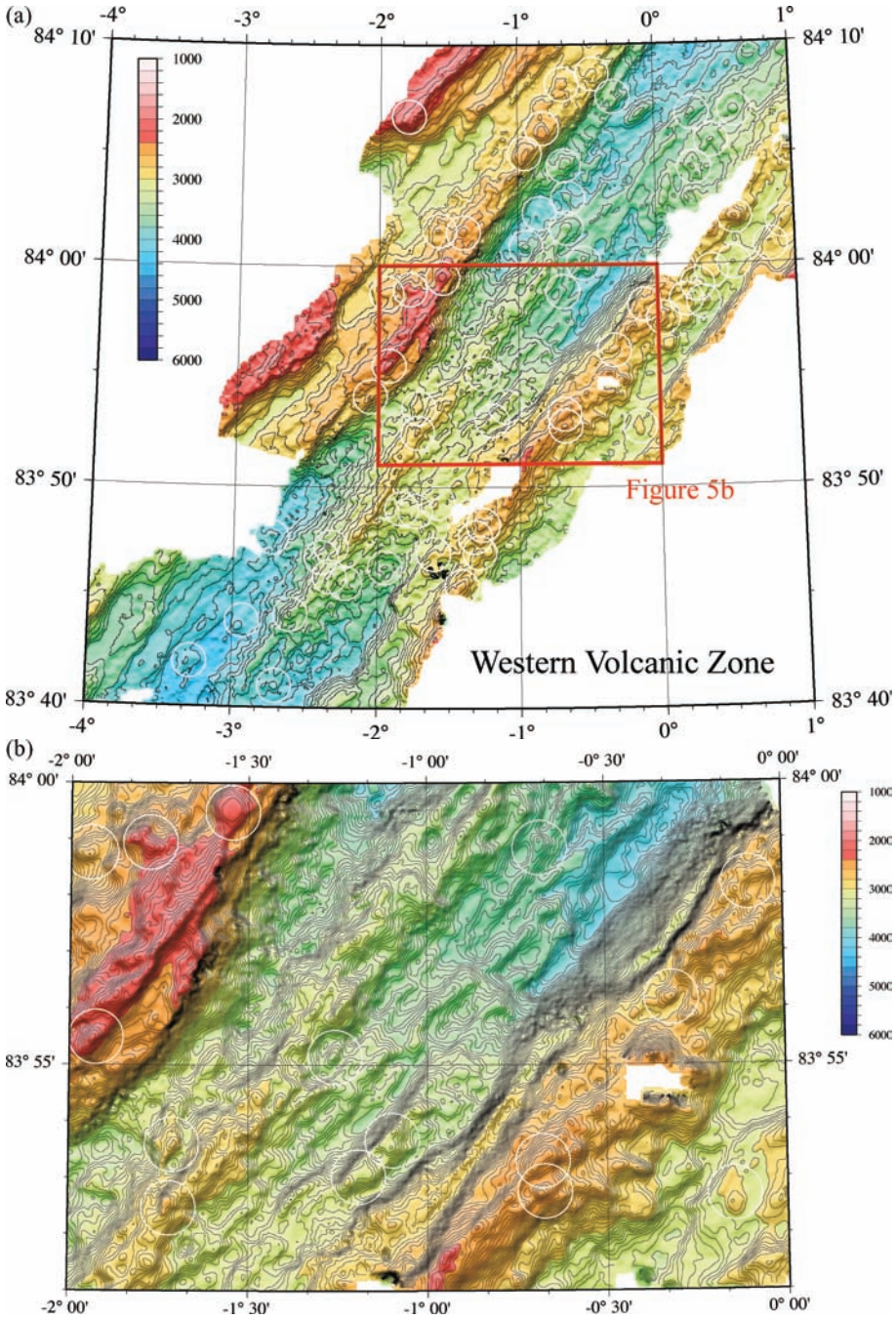

Figure 5. (a) Bathymetry map of the Gakkel Ridge axis from 83°40′N to 84°10′N based on AMORE data (Michael *et al.* 2003). Location of the area within the WVZ is shown in Fig. 2. Map is contoured at 100 m intervals and is illuminated from the northwest. White circles show location of seamounts with height >50 m. Red box outlines the region shown in Fig. 5b. (b) Detailed bathymetry map of a portion of the Gakkel Rift valley within the WVZ. Location is shown in (a). Map is contoured at 20 m intervals and is illuminated from the northwest. White circles show the location of seamounts with height >50 m identified in the region.

generally remains very deep (4700–5400 m) throughout the SMZ (Figs 3a and b), with no systematic pattern of depth variations. The valley floor is very narrow (< ∼5–8 km across) and is generally either flat or concave downward with very few obviously volcanic features (Figs 6a and b). The only areas of volcanic activity identified within the SMZ are near 13°E and 19°E, where Michael *et al.* (2003) recovered basaltic rocks and which are the only areas of bright returns within the EVZ in the SCICEX sidescan data (Fig. 7, Cochran *et al.* 2003).

Michael *et al.* (2003) refer to an elongate ridge extending for ∼20 km along the axis and reaching a depth of 4000 m (Figs 3a and b, 8—profile A) as a volcanic edifice. Unlike the volcanic centres of the WVZ, it is not associated with a shallowing of the rift valley. It sits on the deep rift valley floor, which remains at a depth of 5000 m at the location of the ridge (Fig. 8—profile A). Cochran *et al.* (2003) interpreted this ridge as a tectonic rather than a volcanic feature, based on morphology. They attribute the high backscatter in the region to flows from two rounded bathymetric highs on the north

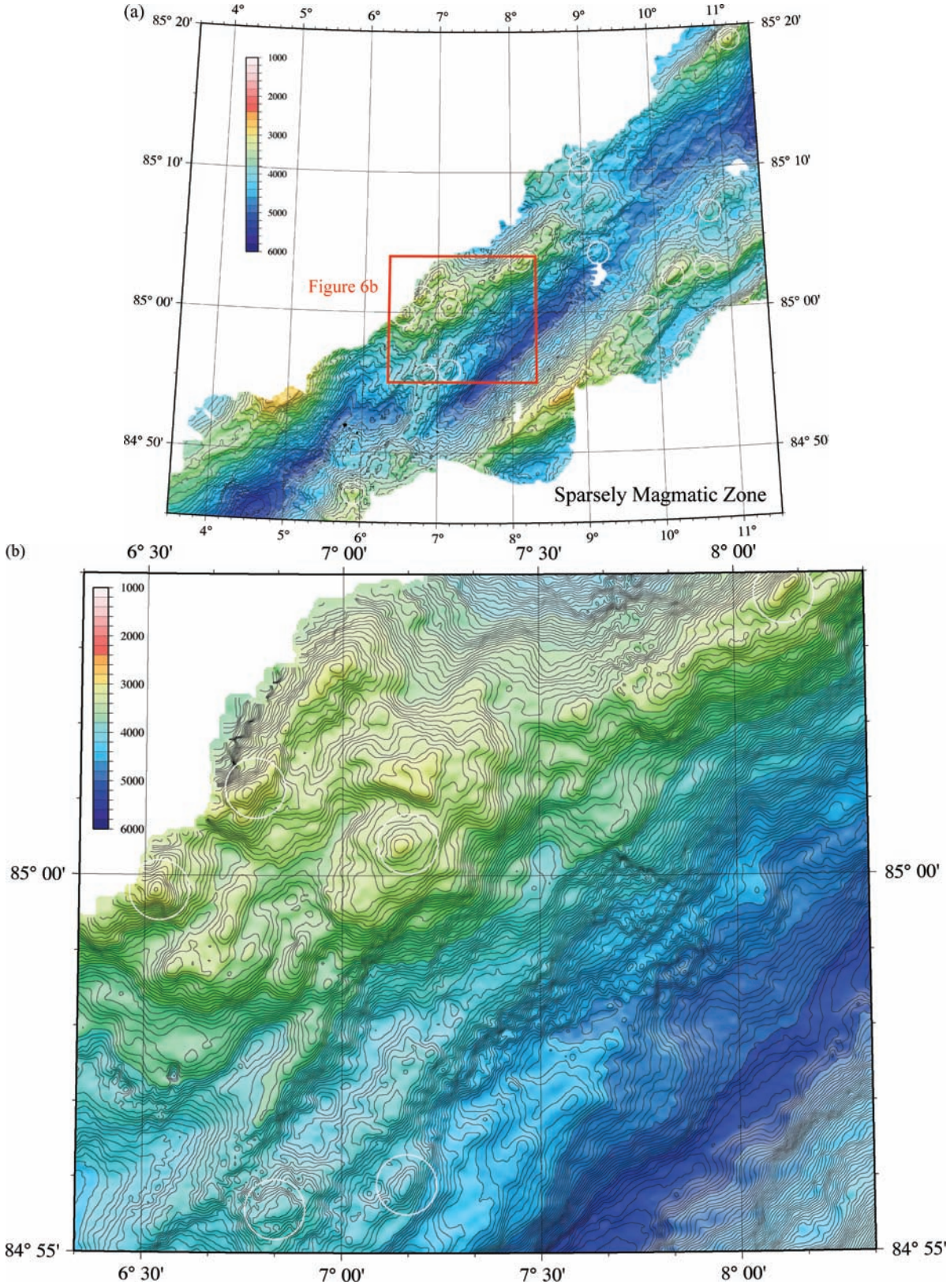

Figure 6. (a) Bathymetry map of the Gakkel Ridge axis from 3°30′E to 11°30′E based on AMORE data (Michael *et al.* 2003). Location of the area within the SMZ is shown in Fig. 3a. Map is contoured at 100 m intervals and is illuminated from the northwest. White circles show location of seamounts with height >50 m. Red box outlines the region shown in (b). Note the lack of seamounts on the valley floor. (b) Detailed bathymetry map of a portion of the Gakkel rift valley within the SMZ. Location is shown in (a). Map is contoured at 20 m intervals and is illuminated from the northwest. White circles show the location of seamounts with height >50 m identified in the region. All of the seamounts are located on the rift valley wall and flanks. Some of these features, such as those near 85°01′N, 6°45′E and 85°03.8′N, 8°08′E are probably of tectonic origin, but others appear to be volcanic.

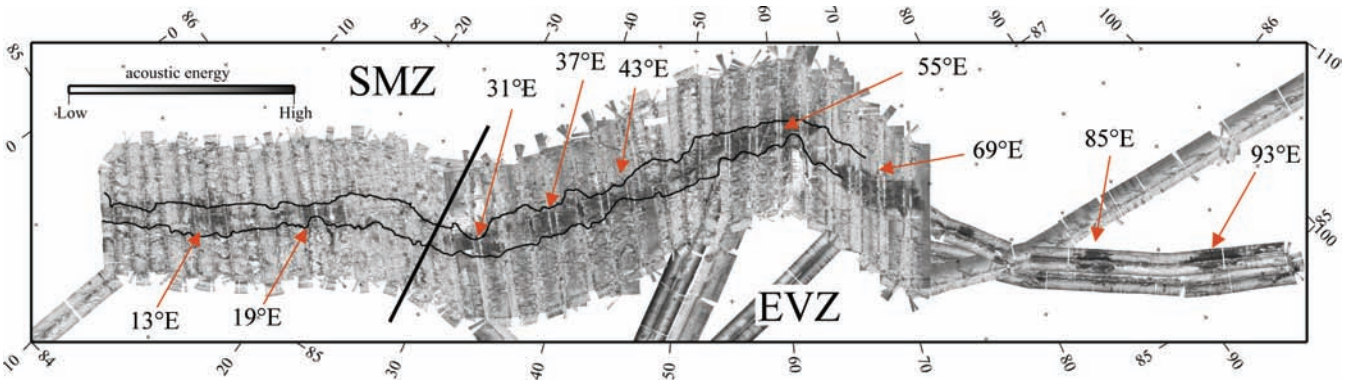

Figure 7. Side scan data from the Gakkel Ridge obtained by USS Hawkbill during the 1998 and 1999 SCICEX cruises (Cochran *et al.* 2003). Black represents very high-energy returns and white represents very low-energy returns. High-energy, or 'bright', returns generally result from the presence of steep slopes or recent volcanic features with little or no sediment cover. Red arrows show the location of volcanic centres within the rift valley. Heavy black line marks the SMZ/EVZ boundary.

flank of the rift valley, which they interpret as volcanoes, although Michael *et al.* (2003) recovered peridotite from the rift valley wall below one of them.

The 19°E volcanic centre is very different. This feature is not a volcanic ridge, but rather a shallowing of the entire rift valley to about 3500 m (Fig. 8—profile D). It is also the site of a prominent across-axis ridge (Fig. 3b), which gravity data imply is associated with 2–3 km of crustal thickening (Cochran *et al.* 2003). Cochran *et al.* (2003) suggested that this might be the only location in their survey area (east of 8°E) where 'typical' oceanic crust, including gabbroic layer 3 has been generated. All rock samples from the 19°E area are basaltic (Michael *et al.* 2003).

Minimum depths in the rift mountains are generally in the range of 2700–3300 m throughout the SMZ, so, rift valley relief is usually in the range of 1500–2200 m (Figs 3b and 8—profiles A–F). Michael *et al.* (2003) note that the transition between the WVZ and SMZ near 3°E is accompanied by a change in the nature of the rift valley walls from sets of high angle faults in the west to large lower angle faults to the east. The slope of the first major scarp south of the axis on six SCICEX lines between 12°40′E and 18°E, measuring the portion of the wall that appears to be a single fault surface at the resolution of the data, ranges from 13° to 19°. The vertical relief on these individual scarps is from 700 to 2300 m (Fig. 8—profiles A–C).

SCICEX data show that the rift mountains are asymmetric to the west of the 19°N volcanic centre. The southern flank consists of a series of high, narrow linear ridges separated by troughs that often are deeper than 4000 m, whereas the north flank has a more massive, blocky structure with less relief (Fig. 8—profiles A–C). Such asymmetry is not apparent east of 19°E. Lineated ridges are still present there (Fig. 3b) but are not separated by deep troughs giving the rift mountains a blockier appearance (Fig. 8—profiles E, F).

Eastern Volcanic Zone

The 'Eastern Volcanic Zone' (EVZ) extends for at least 580 km from about 29°E eastward as far as the axis has been surveyed (∼96°E). This study will be limited to the portion of the EVZ from 29°E to 73°E, where the rift valley is not inundated with sediments and we have good bathymetric coverage (Figs 4a and b).

Although referred to as a 'volcanic zone' by Michael *et al.* (2003), the EVZ is very different from the MAR-like WVZ. The EVZ is characterized by a very deep (∼ 5000 m) rift valley. A series of large volcanic structures are spaced along the rift valley floor at 31°E, 37°E, 43°E, 55°E and 69°E within the well-surveyed portion of the axis (Figs 4a and b). The rift valley is nearly buried by sediments east of the large 69°E volcanic centre (Fig. 8—profile P). However, at least two more volcanic centres have been identified protruding through the sediments near 85°E and 93°E (Edwards *et al.* 2001) and SCICEX sidescan data suggest the presence of at least two more centres between 69°E and 85°E (M. Edwards, private communication, 2007; also see Fig. 7). The volcanic centres typically extend for about 30 km along the axis and reach depths of less than 3500 m (e.g. Fig. 9a). The five volcanic centres to the west of 69°E are each associated with a 20–40 mGal mantle Bouguer (MBA) gravity low (Cochran *et al.* 2003).

A major difference between the EVZ and the SMZ is that SCICEX sidescan data (Fig. 7) shows bright returns, suggesting recent volcanism, along the entire length of the rift valley floor from 29°E to 63°E (Cochran *et al.* 2003). This observation holds even through the ∼85 km stretch of very deep (5000 m), nearly flat rift valley between the 43°E and 55°E centres. This inference is consistent with the observation that all but one dredge from the EVZ recovered basalt, whether the dredges were located on the volcanic highs or in the deep regions between them (Michael *et al.* 2003).

The ridge flanks in the EVZ are generally at a depth of 3000–3500 m with individual ridges having a relief of 500–700 m (Figs 4b and 8—profiles G–P). Although total relief from the rift valley floor to the rift mountains is often 1500–2000 m, the large-offset low angle faults characteristic of the western portion of the SMZ (Fig. 3b and 8—profiles A–C) are not observed in the EVZ.

Distinct changes in the trend of the ridge axis occur near 30°E and 62°E. At each location, a high-standing ridge extends away from the axis on the 'inside corner' (Figs 4b and 8—profiles G, M). Langseth Ridge, the inside corner ridge at 62°E, reaches to within 800 m of the sea surface. These ridges do not have MBA gravity lows and are not areas of thickened crust (Cochran *et al.* 2003). In addition, only altered diabase was recovered from the flanks of these ridges (Michael *et al.* 2003). Both Cochran *et al.* (2003) and Michael *et al.* (2003) suggest that these two ridges are primarily of tectonic rather than volcanic origin.

METHODS

The objective of the bathymetry analysis is to identify and characterize volcanic activity along the Gakkel Ridge in a quantitative and objective manner. We wish to determine how the number, form,

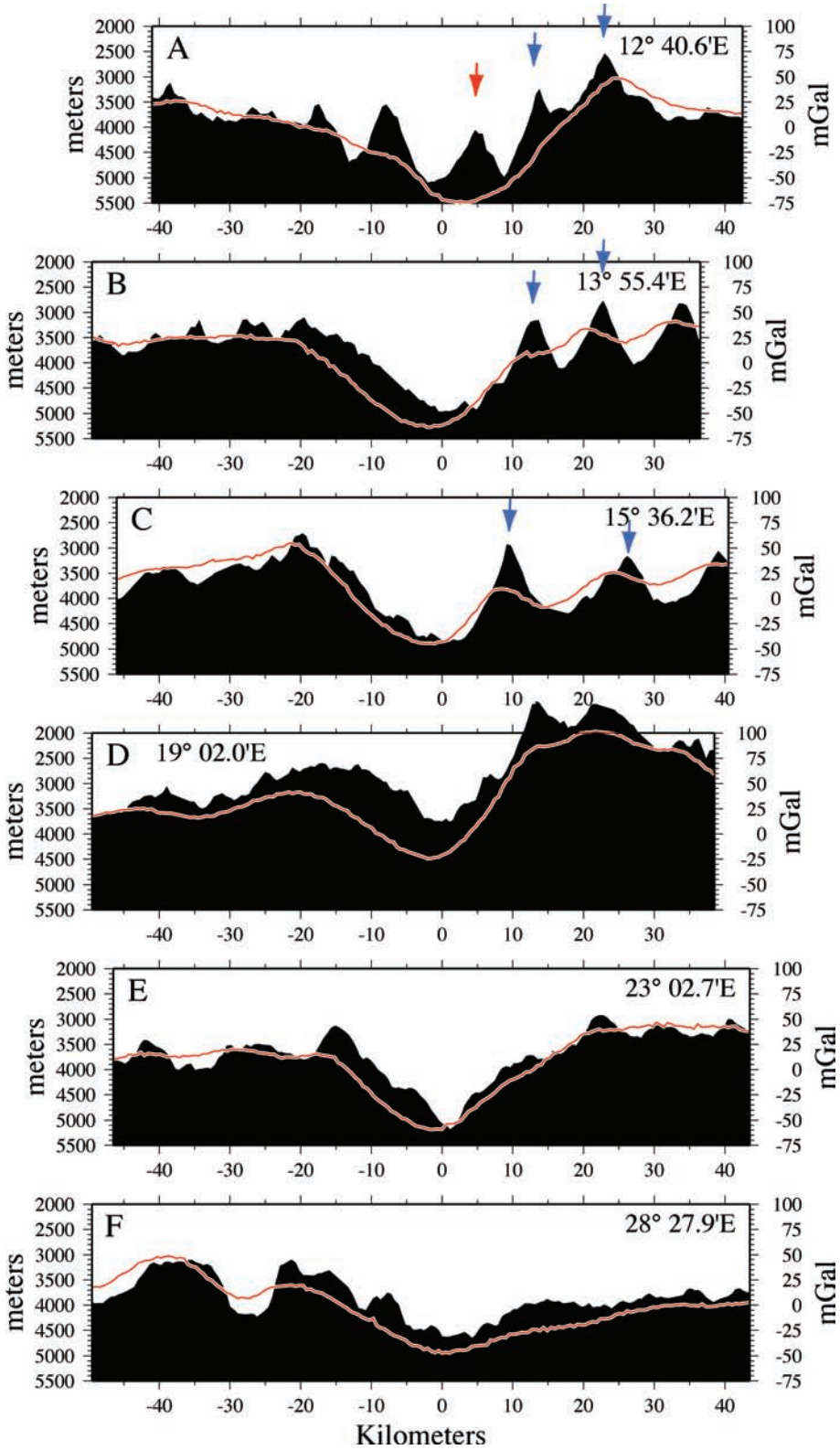

Figure 8. (a) Bathymetry and free-water gravity profiles across the Sparsely Magmatic Zone. Profiles are projected along the local spreading direction with the axis as the origin. North is to the left-hand side (negative distances). The longitude at which each profile crosses the axis is noted. Letters on each profile correspond to those on Fig. 3b, which shows the locations of the profiles. Red arrow identifies the 13°E volcanic centre of Michael *et al.* (2003). Blue arrows identify the high, narrow ridges bounded by low angle faults, which are analogous to the 'smooth terrain' described by Cannat *et al.* (2006) on the SWIR. (b) Bathymetry and free-water gravity profiles across the Eastern Volcanic Zone. Profiles are projected along the local spreading direction with the axis as the origin. North is to the left-hand side (negative distances). The longitude at which each profile crosses the axis is noted. Letters on each profile correspond to those on Fig. 4b, which shows the locations of the profiles.

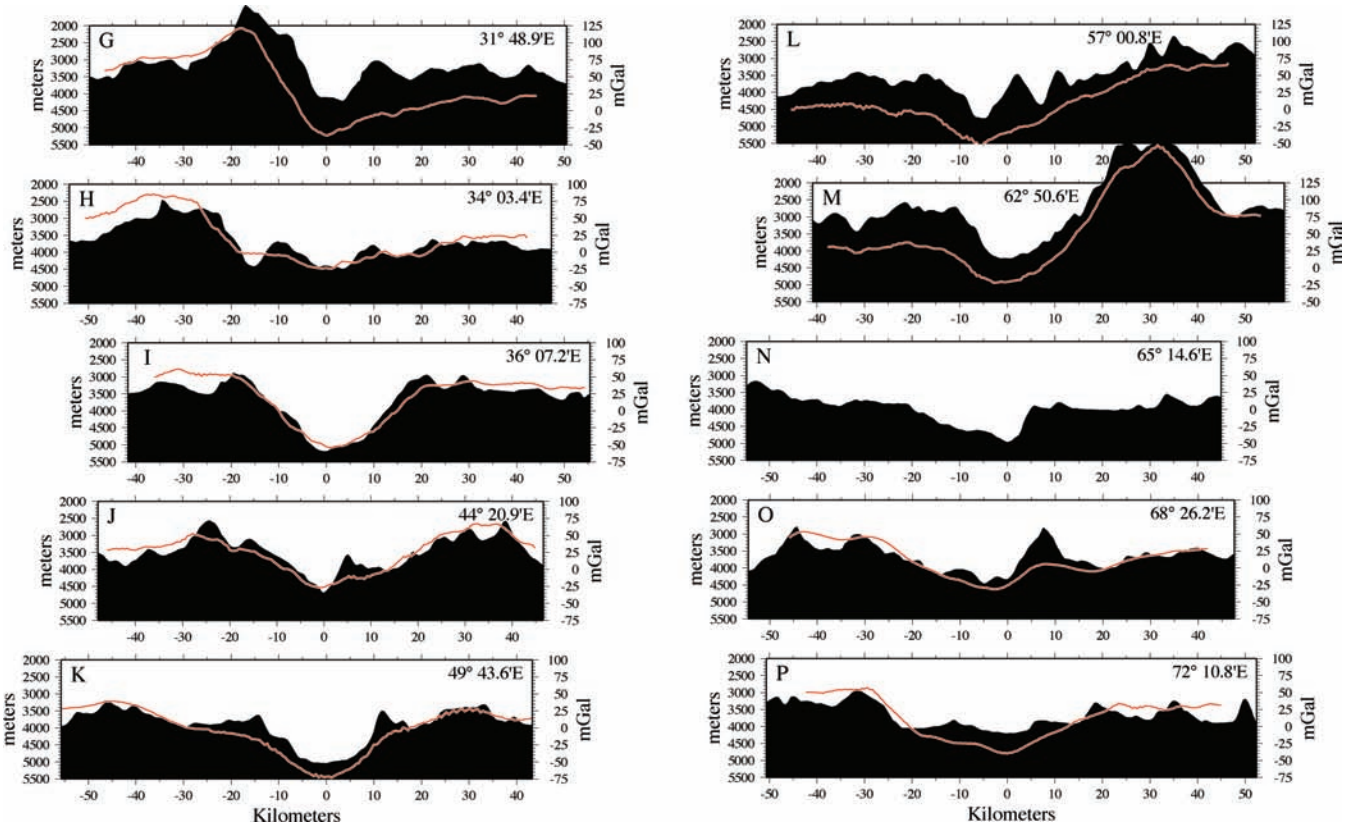

Figure 8. (*Continued.*)

size and distribution of volcanic features varies along the axis and how the volcanism is related to the tectonics and morphology of the ridge axis. In particular, we will examine variations in volcanism between the three magmatic provinces identified by Michael *et al.* (2003). A slightly modified version of a numerical algorithm developed by Behn *et al.* (2004) was used to efficiently and objectively locate volcanoes. The algorithm searches gridded bathymetry data for closed concentric contours with a defined maximum perimeter that delineate a region shallower than the surrounding seafloor. The routine returns the location, height, volume and ellipticity of each feature. The data used for the analysis was the AMORE swath bathymetry gridded with 50-m grid spacing. A contour interval of 20 m was used for the analysis. Behn *et al.* (2004) found that results are insensitive to the choice of contour interval in the range of 10–25 m.

A maximum aspect ratio condition was applied to distinguish volcanic seamounts from elongated topographic highs associated with faulting. The aspect ratio, α, was estimated for each bathymetric feature by fitting an ellipse to the basal contour and determining the principal axes. Only features with α less than a prescribed $\alpha_{\max}$ were identified as volcanic. We found that setting $\alpha_{\max} = 2.5$ generally served to separate volcanic from tectonic features.

The seamount location algorithm provides information on the location, size and shape of the individual volcanic features. The population of seamounts in various regions was characterized by parameters calculated using the maximum likelihood model of Smith & Jordan (1988). Jordan *et al.* (1983) found that the distribution of seamount heights is not Gaussian rather follows an exponential distribution. Therefore, least-squares is not an appropriate method to characterize a set of data. Maximum likelihood (Smith & Jordan 1988) is basically a curve fitting technique that is appropriate for an exponential distribution. It assumes the number, ν, of seamounts per unit area with height > H is given by

$$\nu(\mathrm{H}) = \nu_0 \exp(-\beta \mathrm{H})$$

where ν_0 is the average number of seamounts per unit area and β^{-1} is defined as the characteristic height of the population. The maximum likelihood technique formally determines the best fitting values of ν_0 and β for a set of observed data and the uncertainties in these estimates.

We tested and calibrated our seamount identification technique by identifying seamounts on the MAR from 24°N to 30°N. This is a well-studied area (e.g. Lin *et al.* 1990; Sempere *et al.* 1990) in which similar analyses have been carried out (Smith & Cann 1990, 1992; Behn *et al.* 2004). Fig. 10(a) shows the location of volcanoes identified by our analysis for the central portion (26°N–28°N) of the analysed region. Smith & Cann (1990, 1992) limited their study to seamounts identified on the inner valley floor, defined as the area between the first major fault scarps (usually greater than ~200 m) of the two valley walls, to avoid to minimize the effects of faulting. Our algorithm systematically searches the entire region and identifies features both on the valley floor (shown as white dots) and on the valley walls and flanks (shown as yellow dots). Both the inner floor seamounts and the entire population were analysed to determine differences between the two data sets.

Fig. 10(b) shows the cumulative distribution of volcanoes that we identified on the axial valley floor (bottom) and within the entire studied area marked by the white boxes in Fig. 10(a) (top panels) for the MAR from 24°N to 30°N. The solid line on each plot is the maximum likelihood fit to the distribution of heights. It can be seen that the data fall very close to an exponential distribution to a height of about 300 m. Inherent randomness in the height distribution of

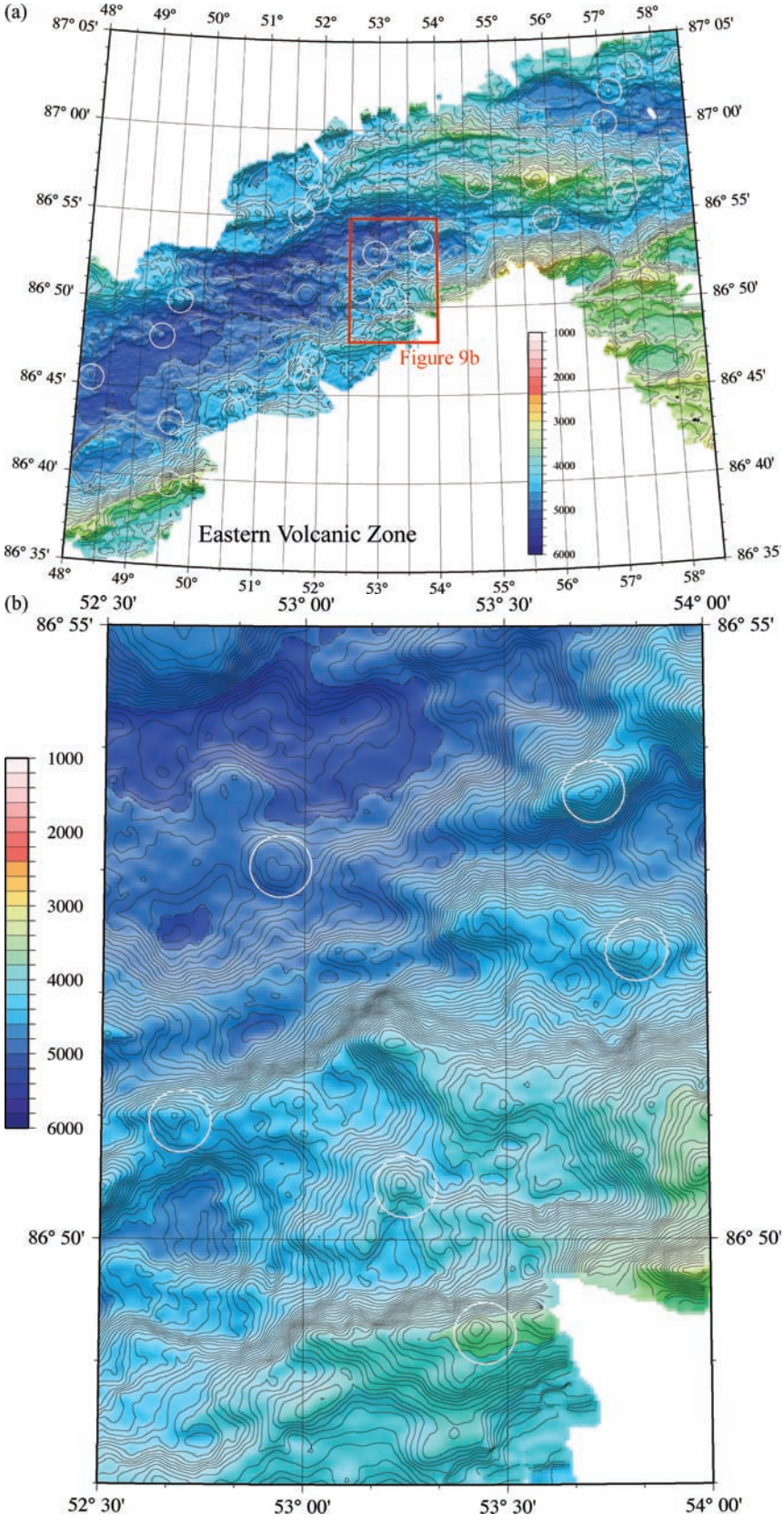

Figure 9. (a) Bathymetry map of the Gakkel Ridge axis from 48°E to 58°30′E in the vicinity of the 55°E volcanic centre based on AMORE data (Michael *et al.* 2003). Location of the area within the EVZ is shown in Fig. 4a. Map is contoured at 100 m intervals and is illuminated from the northwest. White circles show location of seamounts with height >50 m. Red box outlines the region shown in (b). (b) Detailed bathymetry map of a portion of the Gakkel Rift valley within the EVZ. Location is shown in (a). Map is contoured at 20 m intervals and is illuminated from the northwest. White circles show the location of seamounts with height >50 m identified in the region.

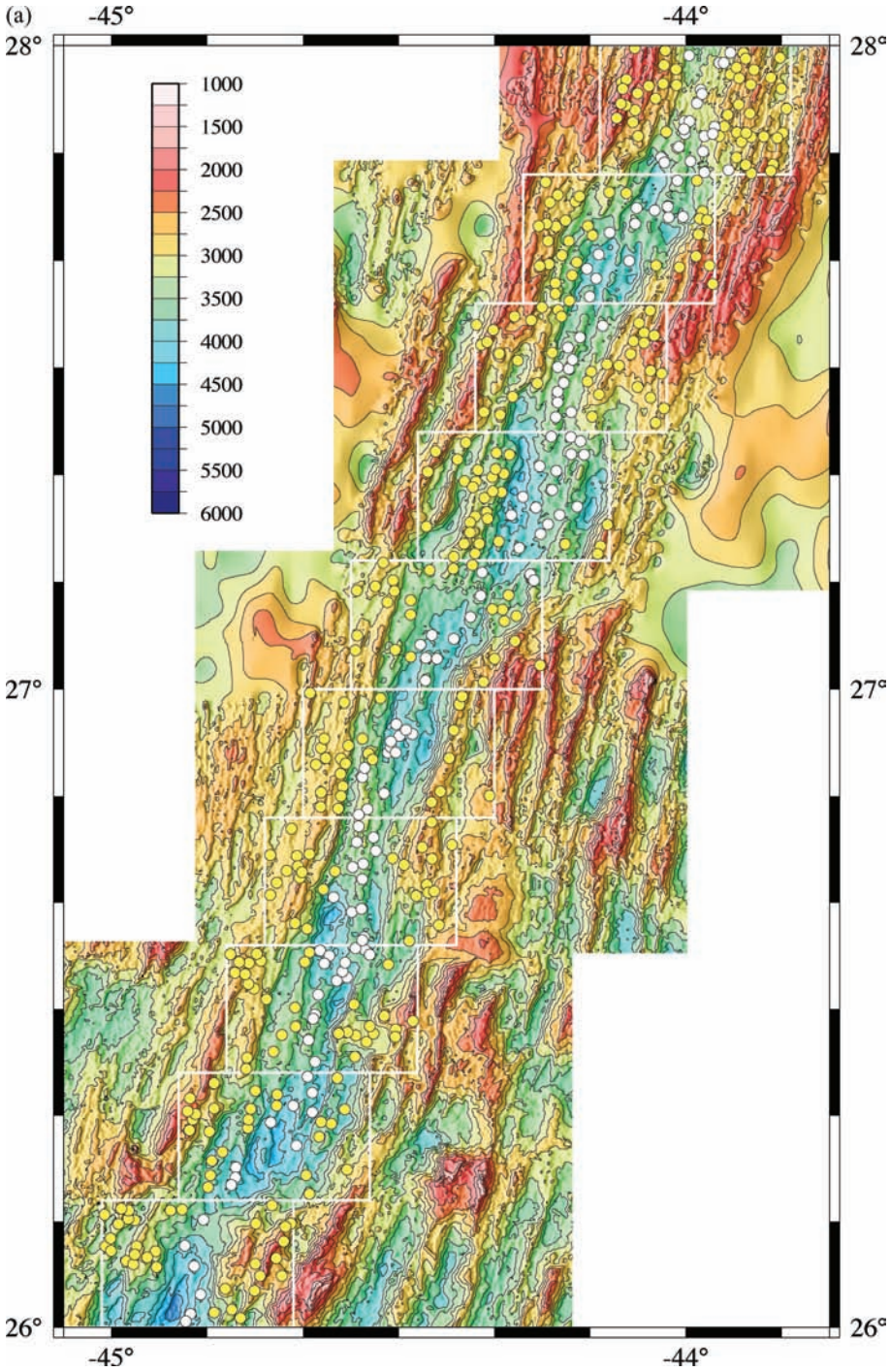

Figure 10. (a) Bathymetry map of the Mid-Atlantic Ridge axis between 26°N and 28°N. White boxes outline areas searched for seamounts. White dots show the location of seamounts identified with height >50 m on the rift valley floor and yellow dots show the location of seamounts on the valley walls and flanks. Map is based on gridded multibeam data where available and bathymetry obtained from satellite data (Smith & Sandwell 1997) elsewhere. Seamount search utilized only shipboard data. Map is contoured at 250 m intervals. (b) Cumulative count of seamounts plotted against height for the Mid-Atlantic Ridge axis from 24°N to 30°N plotted on a linear (left-hand panel) and log (right-hand panel) scale. Solid line shows the maximum likelihood fit to the data. The upper set of plots shows results for the entire region searched and the lower set of plots shows results for the rift valley floor.

the small number of large volcanoes becomes apparent in the log plot at greater heights.

In a maximum likelihood analysis, β defines the slope of the best fitting line in the plot of log(seamount count) versus seamount height and is thus related to the distribution of volcano heights (smaller β implies relatively more large volcanoes). As mentioned above, $1/\beta$, which has units of metres, is defined as the characteristic height of the distribution. We obtained characteristic heights of 42.1 $\pm$ 1.6 m for seamounts on the valley floor and 39.8 $\pm$ 0.8 m for the total population of seamounts on the MAR axis from 24°N to 30°N. This is essentially the same as the characteristic height of 40 $\pm$ 2 m obtained by Behn *et al.* (2004) for the same portion of the MAR.

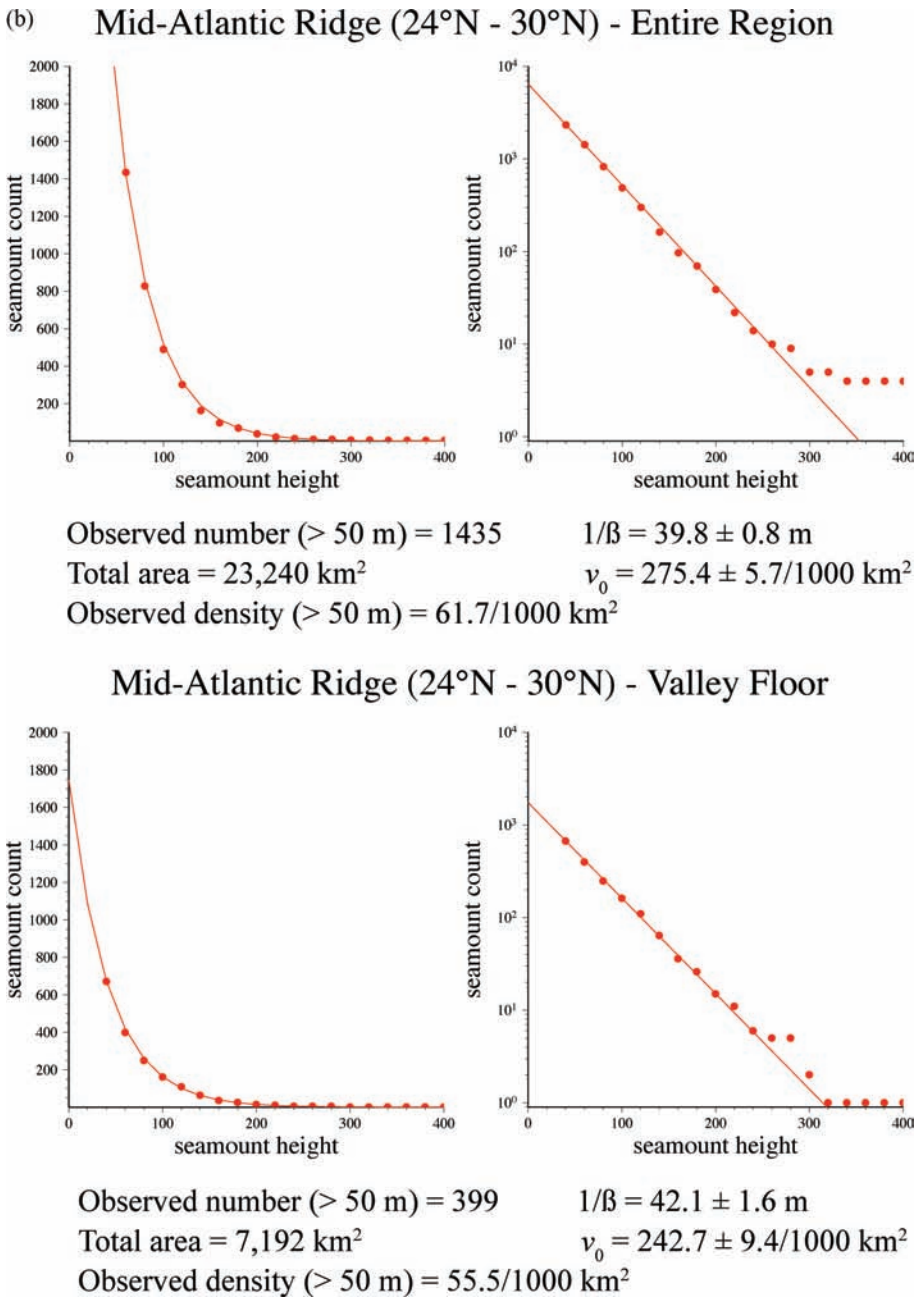

Figure 10. (*Continued*.)

The parameter v_0 is the y-intercept of the maximum likelihood fit to the data (i.e. the total predicted number of seamounts with height greater than 0 m) divided by the area of the region, and provides a measure of the density of volcanic features in the area. However, use of v_0 to characterize the seamount density assumes that there is a plethora of very small volcanoes lurking below the resolution of the mapping system. Although we will determine and report v_0, we will, instead, primarily use the observed density (observed number/area) to characterize the abundance of volcanoes in a region. In doing so, we will count features with relief $h > 50$ m above the surrounding seafloor to be consistent with previous studies (e.g. Batiza *et al.* 1989; Smith & Cann 1990, 1992, 1993; White *et al.* 1998; Behn *et al.* 2004). For the MAR rift valley floor, we identified 399 seamounts with height >50 m and $\alpha < 2.5$ in an area of 7 192 km^2 for an observed density of 55.5 seamounts per 1000 km^2.

The seamount density for the entire region, including the valley walls and flanks, is 61.7 seamounts per 1000 km^2 (1435 seamounts in 23 240 km^2). The 10% higher density for the entire region might just represent random fluctuation, or it might be the result of identifying tectonic features as seamounts on the valley flanks. Statistical analysis of the Gakkel Ridge data will be based on seamounts identified on the rift valley floor.

RESULTS

Western Volcanic Zone

Fig. 2 shows the location of seamounts with relief >50 m above the surrounding seafloor identified along the axis of the WVZ. The analysis identified 76 seamounts on the rift valley floor within an

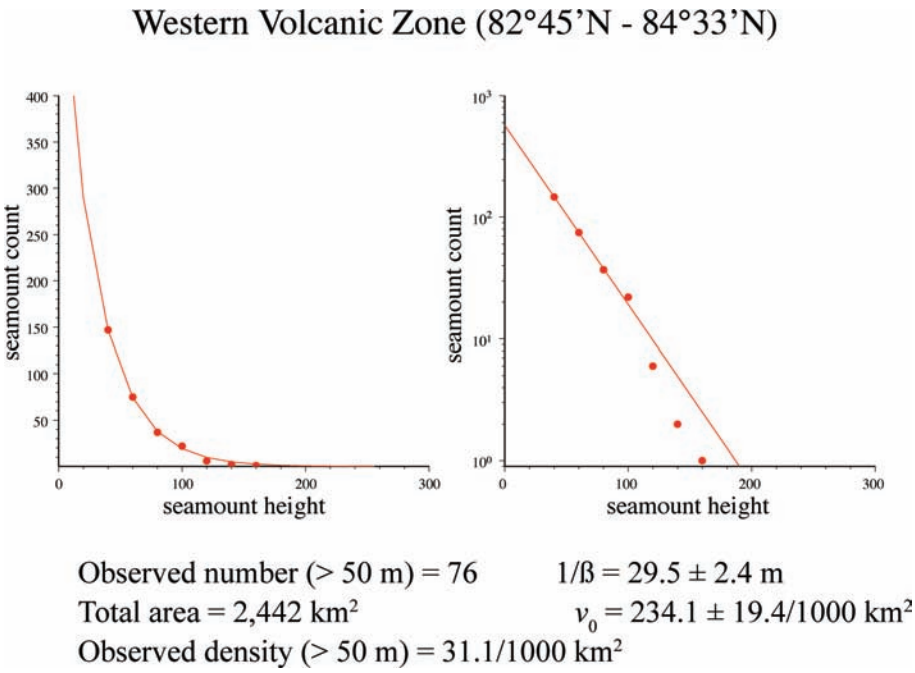

Figure 11. Cumulative count of seamounts on the rift valley floor plotted against height for the Western Volcanic Zone on a linear (left-hand panel) and log (right-hand panel) scale. Solid lines show the maximum likelihood fit to the data. Fig. 2 shows the location of seamounts with height >50 m.

area of 2442 km^2 for an observed average density of 31.1 seamounts per 1000 km^2, which is roughly 55% of the density observed at the MAR rift valley floor. The characteristic height of the WVZ seamounts is 29.5 m (Fig. 11). Thus, not only there are significantly fewer seamounts per unit area observed in the WVZ than at the MAR but they are also considerably smaller. The smaller size of volcanic features is evident by the observation that there are no seamounts in the WVZ taller than 170 m (Fig. 11), whereas 36 seamounts (9.2% of the total population) are taller than 170 m on the rift valley floor in the studied portion of the MAR, with seamounts as high as 460 m observed. With a similar height distribution, seven seamounts taller than 170 m would be expected in the WVZ.

Both the axial morphology and the distribution of volcanoes are not uniform along the WVZ axis. Morphologically, the four prominent axial bathymetric highs are located south of about 84°N (Fig. 2), whereas relief along the rift valley floor is lower to the north of 84°N. Fig. 12 shows the seamount density for each of the computational boxes along the WVZ along with an axial depth profile. The region north of 83°45′N has a greater concentration of volcanic seamounts than does the southern portion of the WVZ. Fig. 13 shows the results of performing separate maximum likelihood analyses of the southern region from 82°57′N to 83°45′N and the northern region from 83°45′N to 84°33′N. The area south of 82°57′N was not included because it is primarily occupied by the northern end of the Lena Trough, a deep, obliquely opening and nearly amagmatic portion of the plate boundary (Snow *et al.* 2001; Hellebrand & Snow 2003). The southern region has a seamount density of 22.6 per 1000 km^2 and a characteristic height ($1/\beta$) of 26.9 m. The density of volcanoes in this area is 40% of that of the portion of the MAR that we examined and the individual volcanoes are much smaller. In the northern region, the seamount density is 52.3 per 1000 m^2 with $1/\beta = 31.4$ m. In this portion of the WVZ, the density of seamounts approaches that of the MAR. However, the individual volcanoes are still much smaller and represent significantly less erupted magma than volcanoes at the MAR.

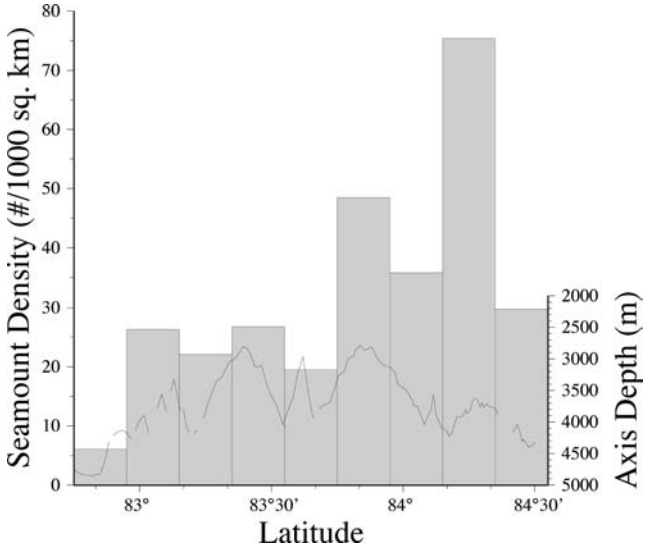

Figure 12. Bar graph of the observed density of valley floor seamounts with height >50 m within each of the computational boxes in the Western Volcanic Zone. Width of each bar corresponds to the latitude range of the box as noted on the horizontal axis. Location of boxes is shown in Fig. 2. Solid line is a profile of the axial depth within the WVZ.

Sparsely Magmatic Zone

The locations of seamounts with $h > 50$ m from within the SMZ rift valley are plotted on Fig. 3(a). There are nine seamounts exceeding 50 m in height identified on the valley floor in an area of 1 390 km^2 for an observed seamount density of 6.5 per 1000 km^2. The small number of volcanic features in this region precludes meaningful statistical analysis. It is apparent from Fig. 3(a) that there is a concentration of volcanic features in the vicinity of the 19°E magmatic centre. The observed seamount density in the region of the

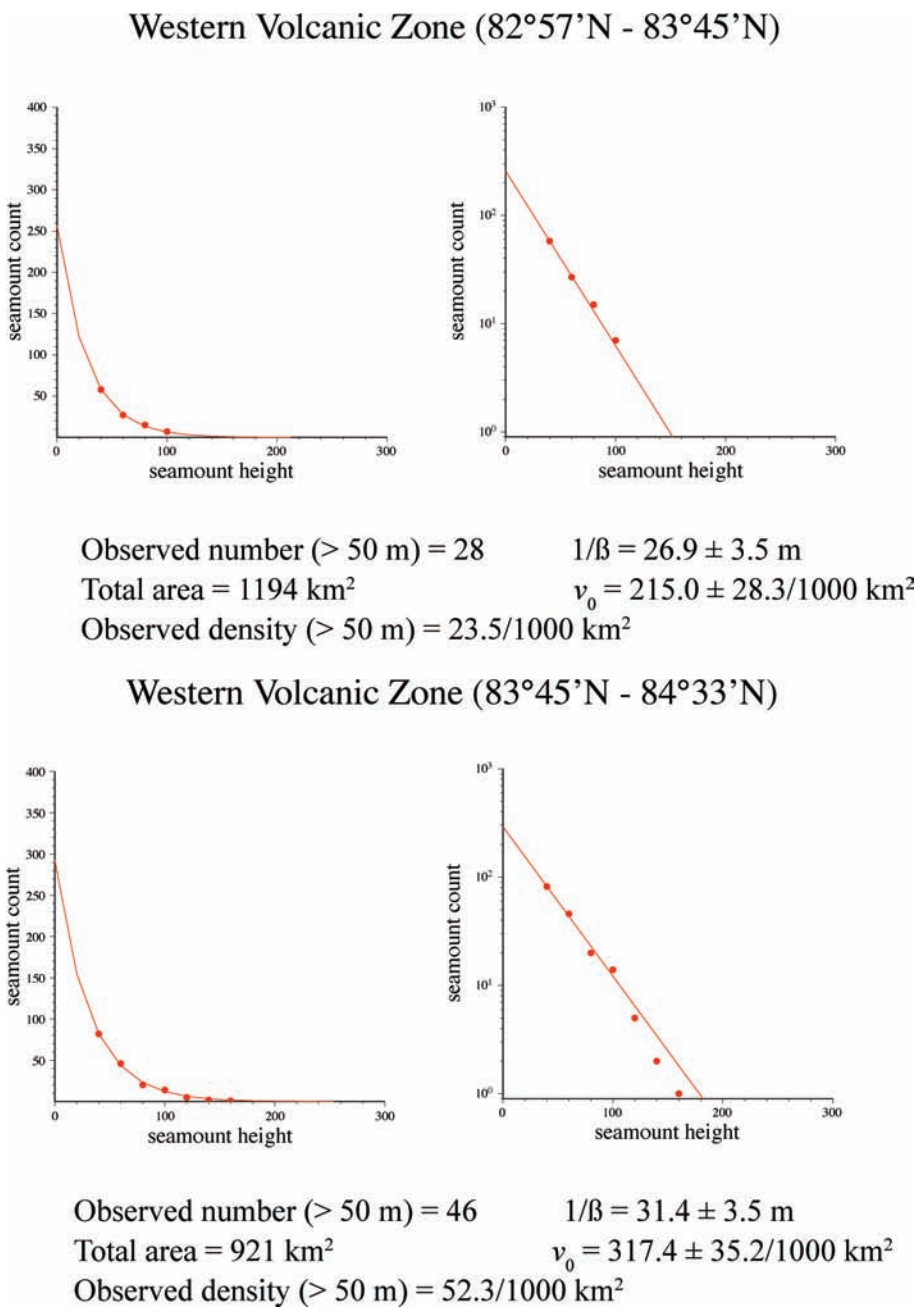

Figure 13. Cumulative count of seamounts on the rift valley floor plotted against height for the Western Volcanic Zone from 82°57′N to 83°45′N (top panel) and from 83°45′N to 84°33′N (bottom panel). In each area, the data is plotted on a linear (left-hand panel) and log (right-hand panel) scale. Solid lines show the maximum likelihood fit to the data. Fig. 2 shows the location of seamounts with height >50 m.

magmatic centre is 20.8 per 1000 km^2. The concentration of seamounts at 19°E is similar to that in the southern part of the WVZ, but the 19°E seamounts appear to be somewhat shorter (the tallest is 80 m high).

If the 19°E magmatic centre is excluded, the observed seamount density drops to 2.7 per 1000 km^2 with only three seamounts more than 50 m high observed in an area of 1101 m^2. All three of these are east of 26°E, in the eastern 25 km of the WMZ as defined by Michael *et al.* (2003). In particular, there are no seamounts taller than 50 m on the rift valley floor for over 185 km to the southwest of 17°35′E, including the entire SMZ to the west of the 19°E magmatic complex. There are 14 smaller features between 20 and 50 m high identified in this region. Some of these may well be artefacts in the swath bathymetry (features were not edited out unless undoubtedly an artefact), but there clearly are some very small seamounts, particularly near 14°E and to the east of 16°E near the 19°E complex. These are near the edges, rather than in the centre, of the valley floor.

Eastern Volcanic Zone

The locations of seamounts with $h > 50$ m within the EVZ are plotted in Fig. 4(a). A total of 62 seamounts were identified in an area of 4 296 km^2, giving a density of 14.4 seamounts per 1000 km^2. The characteristic height is 22.9 m (Fig. 14). As found throughout the Gakkel Ridge, individual volcanic structures are significantly

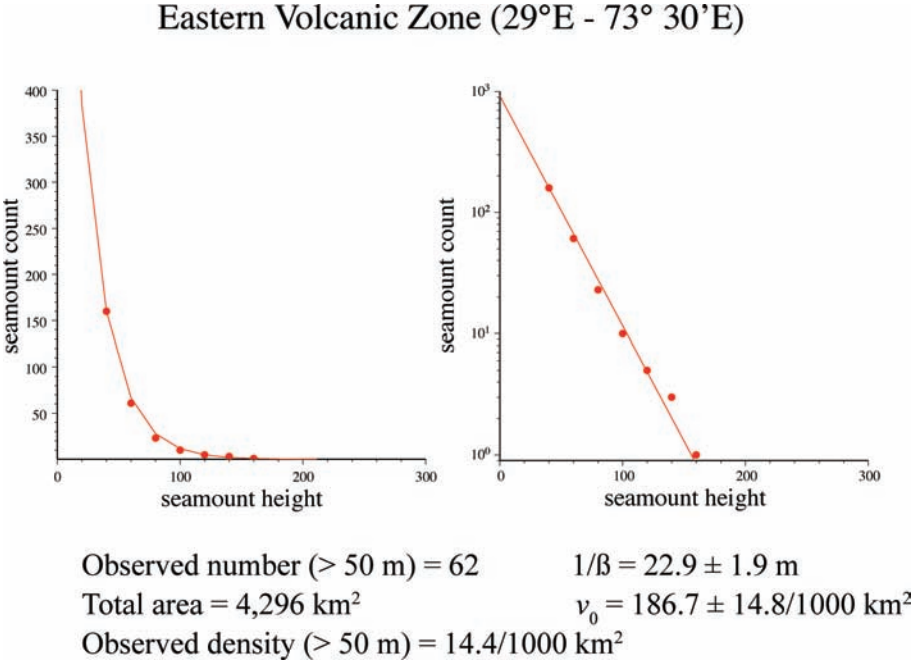

Figure 14. Cumulative count of seamounts on the rift valley floor plotted against height for the Eastern Volcanic Zone plotted on a linear (left-hand panel) and log (right-hand panel) scale. Solid lines show the maximum likelihood fit to the data. Fig. 4a shows the location of seamounts with height >w50 m.

smaller than observed at the MAR. The seamount concentration is significantly greater than in the SMZ, but is less than observed in the WVZ. There is a clear tendency for volcanic structures to cluster on the large volcanic centres (Fig. 4a). However, seamounts are observed along the entire length of the EVZ. As in the SMZ, most of the seamounts away the volcanic centres are located near the edge of the rift valley floor (Fig. 4a).

The presence of volcanic features between the large volcanic features is consistent with the observation that SCICEX sidescan data show bright returns (Fig. 7), suggesting recent volcanism, along the entire rift valley floor (Cochran *et al.* 2003). In addition, basalt was recovered from all but one dredge in the EVZ during the AMORE expedition, whether the dredge was located on the magmatic centres or in the areas of deep rift valley between them (Michael *et al.* 2003), and seismic refraction data show a thin, low-velocity 'crustal' layer (Jokat & Schmidt-Aursch 2007). Thus, although the rift valley floor in the SMZ is primarily peridotite, at least a veneer of basalt appears to be present throughout most of the EVZ.

DISCUSSION

Although the western and eastern sections of the surveyed portion of the Gakkel Ridge are both referred to as 'volcanic zones', they display two very different patterns of magmatism and tectonics.

Western Volcanic Zone

The WVZ has been described as magmatically robust with 'abundant' volcanism (e.g. Michael *et al.* 2003; Baker *et al.* 2004) due largely to its morphologic similarity to the MAR (Figs 2, 5 and 10a). Smith & Cann (1990, 1992, 1993) have shown that the basic extrusive volcanic unit of the MAR is localized, point-source (seamount) volcanoes, probably fed by dykes injected along the axis (e.g. Smith & Cann 1999; Magde *et al.* 2000; Hussenoeder *et al.* 2002; Dunn *et al.* 2005). The number of such structures per unit area at the WVZ is 55% of that at the 24°N–30°N region of the MAR axis (Figs 2 and 10a). In addition, volcanic edifices along the WVZ are significantly shorter than those observed at the MAR (Figs 10b and 11) and thus contain an appreciably smaller volume of erupted lava. The low melt production is also reflected in the crustal thickness. Jokat & Schmidt-Aursch (2007) carried out four seismic refraction experiments in the WVZ and obtained crustal thicknesses ranging from 1.2 to 4.9 km with a mean of 2.95 km. The two results that they considered most reliable gave crustal thicknesses of 2.5 and 4.9 km.

Compared with the MAR, the WVZ is therefore actually magma-poor. However it is a 'genteel' poverty that is able to 'keep up appearances'. Although the surface expression of volcanic activity, and presumably the total melt supply, are drastically curtailed relative to the MAR, the WVZ spreading axis is able to maintain an MAR morphology with axial volcanic ridges, volcanoes scattered about the rift valley floor, and rift valley walls consisting of sets of high-angle normal faults (Fig. 5). Thus, the basic style of melt generation and distribution, and the associated tectonic activity observed on the MAR, can be maintained even at the lowered melt production of the WVZ.

Eastern Volcanic Zone

The EVZ displays an entirely different form of mid-ocean ridge tectonics and crustal generation. It is characterized by large volcanic centres irregularly spaced at 50–150 km intervals along the axis and separated by stretches of deep (~5000 m), low relief valley floor (Figs 4a and 9a). Small volcanic edifices are clustered around the volcanic centres (Fig. 4a). The volcanic centres also coincide with large anomalies on aeromagnetic lines, whereas the axial magnetic anomaly is of lower amplitude and less distinct along the rest of the rift valley (Brozena *et al.* 2003; Jokat *et al.* 2003), supporting the conclusion based on morphology that volcanism is strongly focused at the volcanic centres. Although some degree of focusing

of melt within segments is observed at all spreading rates (e.g. Wang & Cochran 1993, 1995; Detrick *et al.* 1995; Magde *et al.* 2000), focusing of melt to the volcanic centres appears to be exceptionally effective at the EVZ, with nearly all of the melt generated beneath long stretches of the axis transported to the volcanic centres. There also appears to be little redistribution of melt back along the axis by crustal level dykes, as observed at the MAR (Magde *et al.* 2000; Dunn *et al.* 2005).

This form of crustal emplacement probably develops when the lithospheric lid becomes too thick for the melt produced to penetrate, resulting in melt migrating laterally to the volcanic centres. Cochran *et al.* (2003) and Dick *et al.* (2003) both suggested that the volcanic centres developed as the result of melting of a heterogeneous veined mantle, resulting in local mantle diapirism at the site of an inhomogeneity. Once established, the volcanic centres will tend to maintain themselves as low viscosity conduits for melt to the surface.

Volcanic centres in the EVZ typically extend for 20 to 40 km along-axis and are oriented perpendicular to the spreading direction. At the Gakkel Ridge, which is only mildly oblique to the spreading direction, the volcanic centres are contained within the rift valley walls and rest on the valley floor (Figs 4a and 9a). At some portions of the SWIR that are much more oblique to the spreading direction (e.g. at 55°E–56°E), volcanic centres with similar dimensions and gravity signature result in a kinked rift valley with E–W-trending (perpendicular to the spreading direction) volcanic ridge sections alternating with NE–SW trending deep, non-volcanic sections (Sauter *et al.* 2001; Dick *et al.* 2003).

The SWIR geometry led Dick *et al.* (2003) to describe the 'ultraslow' class of ridge axes as consisting of 'linked magmatic and amagmatic accretionary ridge segments'. However, the SWIR volcanic centres are constructed with melt generated beneath the adjacent amagmatic sections and focused to them. Thus, the volcanic centre and adjacent amagmatic portions of the rift valley form a single magmatic unit or segment, even if the SWIR axis is partitioned morphologically into spreading-normal volcanic and highly oblique non-volcanic sections.

The presence of some seamounts in areas of deep rift valley between the volcanic centres (Figs 4a and 9a) as well as bright sidescan returns from much of the valley floor (Fig. 7) and the recovery of basalt in these regions requires that some lava is erupted away from the volcanic centres in the EVZ. The four seismic lines reported from the EVZ (Jokat & Schmidt-Aursch 2007) show very similar crustal thicknesses ranging from 2.6 to 3.3 km with a mean thickness of 2.9 km. These results overlap with the results from the WVZ, but have a lower mean thickness, particularly if stations 171 and 172 from the WVZ, which were noisy and considered to be of poor quality by Jokat & Schmidt-Aursch (2007), are eliminated. However, given the relatively low density of seamounts between the volcanic centres (nine seamounts >50 m high are observed in 85 km of rift valley floor between the 43°E and 55°E complexes and only one seamount is found in the 45 km between the 55°E and 69°E complexes) and their small size (none of those 10 seamounts is over 100 m high and six of them are less than 70 m high), it is unclear how 3 km of basalt can be built-up. Although basalt certainly covers the rift valley floor, it may form a relatively thin veneer with some portion of the low-velocity upper seismic layer made up of altered mantle rocks, as suggested by Jokat & Schmidt-Aursch (2007) for the 'crustal' layer observed in the SMZ.

The observation that seamounts in the deep regions between volcanic centres are primarily at the edges of the valley floor and on the rift valley walls (Figs 4a, 9a and b) suggests that this lava ascends along faults. A similar observation on the role of faults in abetting and determining the location of magmatism was made at the northern Red Sea by Cochran (2005), who noted that the small volcanoes in that region are systematically located along faults bounding large crustal blocks. The northern Red Sea is a late-stage continental rift, which has undergone non-magmatic extension (Bosworth *et al.* 2005) until recently, when small amounts of magma have erupted to form the volcanoes observed by Cochran (2005). It appears that small magma bodies generated beneath a lithospheric lid may use deep penetrating faults as a conduit to the surface in a number of tectonic settings.

Sparsely Magmatic Zone

The SMZ is also characterized by intermittent volcanic centres separated by regions of deep rift valley. The distance between volcanic centres is greater in the SMZ than in the EVZ and there is virtually no volcanism along the deep valley segments. However, the mode of melt focusing and crustal generation appears to be the same as at the EVZ. The extreme focusing of the melt produced in this region to the few large magmatic centres is demonstrated by the observation that the crustal thickness determined from seismic experiments in the SMZ range from 1.4–2.5 km with the mean <2 km (Jokat & Schmidt-Aursch 2007). Jokat & Schmidt-Aursch (2007) suggest that there may be no magmatic crust in much of this area and that the low upper velocities that they determined result from serpentinization of peridotite. This is consistent with the lack of 'bright' returns, indicative of young volcanic rocks, in sidescan data from the ridge axis (Fig. 7).

A unique feature of the SMZ is the series of high, axis-parallel narrow ridges separated by deep troughs that are located on the southern flank to the west of the 19°E volcanic centre (Figs 3b and 8—profiles A–C). These ridges are spaced 10–20 km apart, and their axis-facing side consists of large-offset scarps dipping toward the axis at less than 20°. These features differ from the low-angle 'megamullions' or 'oceanic core complexes' observed at the MAR (e.g. Cann *et al.* 1997; Blackman *et al.* 1998; Tucholke *et al.* 1998) and SWIR (Cannat *et al.* 2006). The total offset on these surfaces is much less than typically observed on oceanic core complexes and the corrugated surface characteristic of the core complexes is not observed. These ridges are analogous to the 'smooth terrain' described by Cannat *et al.* (2006) near 64°E on the SWIR.

Buck *et al.* (2005) used numerical models to investigate variations in the nature of mid-ocean ridge faulting as a function of melt supply as a function of a parameter, M, defined as the fraction of the plate separation accommodated by dyke injection. They found that, for a range of M near 0.5, very large offset faults can develop because the active portion of the fault remains near the axis in the region of weakest lithosphere. Buck *et al.* (2005) identify this situation as a mechanism for the creation of oceanic core complexes. For $M \neq 0.5$, the fault moves off-axis into thicker lithosphere and is then abandoned as a new fault forms near the axis. For large M (a highly magmatic axis), inward-dipping small-offset, high angle normal faults are produced (Buck *et al.* 2005). For small M (an amagmatic axis), relatively large offset (several kilometres) faults can still form but are abandoned as they are transported off axis. In Buck *et al.*'s (2005) numerical models, a series of small offset normal faults developed on the opposite side of the ridge from the large offset faults. This form of periodic formation and abandonment of large-offset faults may be responsible for the characteristic 'smooth' terrain observed at places on the Gakkel and Southwest Indian Ridges.

Modes of crustal generation

Dick *et al.* (2003) have argued that the Gakkel Ridge to the east of 3°E and portions of the SWIR where similar morphology is found constitute a separate 'ultraslow' class of mid-ocean ridge with morphology, crustal structure and magmatic and tectonic patterns that are distinct from those found at higher spreading rates. Our analysis of the number and distribution of seamounts along the Gakkel Ridge is consistent with this conclusion. Very different patterns of volcanic activity are seen at the WVZ and at the rest of the Gakkel Ridge. The WVZ is much less vigorous than the MAR, but maintains an MAR-like appearance and distribution of magmatic features. It appears that a slow-spreading 'MAR-like' form of crustal generation and tectonics resulting in an axial volcanic ridge, small volcanoes scattered on the rift valley floor, and rift valley walls made up of sets of high-angle normal faults can be maintained until the melt supply decreases and the lithospheric lid increases to some critical value. At that point, there is an abrupt change to an entirely different form of 'EVZ-like' axial processes that involve much greater focusing of melt leading to the creation of widely spaced, large magmatic centres separated by areas where there is at best a thin veneer of basalt overlying mantle rocks with volcanoes mainly located on the rift valley walls and fed by melt ascending along faults.

Dick *et al.* (2003) suggest that the transition between the 'slow' and 'ultra-slow' modes of crustal generation occurs at about 12 mm yr^{-1}. They base this on observations at the Gakkel Ridge, where the abrupt transition between the WVZ and the SMZ near 3°E occurs at a spreading rate of 12.2 mm yr^{-1}, and the westernmost portion of the SWIR near 16°E where the transition occurs at an effective spreading rate (component of plate separation perpendicular to the ridge trend) of about 12.4 mm yr^{-1}.

However, as noted in passing by Dick *et al.* (2003), the transition cannot be dependent simply on effective spreading rate. The influence of factors other than spreading rate can be seen at the 3°E transition from 'slow' to 'ultra-slow' morphology on the Gakkel Ridge. An indication that the threshold transition from 'slow' to 'ultraslow' form of axial processes can be caused and localized by factors other than simply spreading rate comes from variation in magmatic activity approaching the 3°E WVZ–SMZ boundary. The number and size of volcanic seamounts in the WVZ does not decrease from southwest to northeast approaching the EVZ. Instead, both parameters increase significantly. This is consistent with seismic refraction data that gives a crustal thickness of 2.5 km profile 190 centred near 83°30′N and 4.9 km for Profile 180 centred just north of 84°N (Jokat & Schmidt-Aursch 2007). Thus, it would appear that the 'vigour' of the magmatic system in the WVZ increases rather than decreases, approaching the 3°E boundary with the SMZ. Similarly, in the SMZ, magmatism does not increase approaching the WVZ. The ridge axis from 3°E to 17°35′E, is the most amagmatic section of axis on the known portion of the Gakkel Ridge, and perhaps in the entire mid-ocean ridge system, with no volcanic features >50 m high observed for the entire 185 km and extensive areas of exposed peridotite. The abrupt transition at 3°E is thus from the most magmatic to the most amagmatic sections of the Gakkel Ridge.

Goldstein *et al.* (2008) identified an abrupt isotopic boundary between 13°E and 16°E in the centre of the SMZ. Lavas recovered to the west of the boundary, including in the WVZ, have isotopic characteristics typical of the 'DUPAL' isotopic anomaly of Indian and South Atlantic MORB (Dupre & Allegre 1983; Hart 1984) while those from east of the boundary are consistent with normal 'Pacific–Atlantic' isotope trends. Goldstein *et al.* (2008) drew an analogy between the isotopic boundary on the Gakkel Ridge and the Australian–Antarctic Discontinuity (AAD) on the Southeast Indian Ridge (SEIR), which is also the site of an abrupt boundary between DUPAL and Pacific mantle provinces (Klein *et al.* 1988, 1991; Pyle *et al.* 1992). The AAD is a very deep area of chaotic morphology (Weissel & Hayes 1974; Palmer *et al.* 1993) characterized by low melt production and thin crust (Anderson *et al.* 1980; Forsyth *et al.* 1987; Kuo 1993; Tolstoy *et al.* 1995). At both the Gakkel Ridge and the SWIR, a sharp, distinct compositional boundary in the mantle occurs within a region where the ridge axis is deep and extremely amagmatic. In addition, the portion of the SEIR immediately to the east of the AAD is one of the most vigorous sections of the SEIR, with a shallow crustal depth and a well-developed 'EPR-like' axial high (West *et al.* 1994). In both of these cases, a sharp boundary between magmatic and extremely amagmatic portions of the ridge axis coincides with a major chemical boundary that occurs within the amagmatic region.

Another example of the influence of parameters other than spreading rate, and in particular discontinuities in mantle composition, in localizing the transition from 'slow' to 'ultra-slow' spreading comes from considering two portions of the SEIR on either side of the Melville transform at 60°45′E. The eastern SWIR, in the vicinity of the Melville transform, is spreading almost exactly N–S at a fairly constant rate of ∼14 mm yr^{-1} (Patriat & Segoufin 1988; DeMets *et al.* 1994; Cannat *et al.* 2003).

The SWIR to the east of the Melville transform is characterized by widely spaced large volcanic centres separated by deep, nearly flat stretches of rift valley (Mendel & Sauter 1997; Mendel *et al.* 2003; Sauter *et al.* 2004; Gomez *et al.* 2006) and appears analogous to the EVZ or SMZ of the Gakkel Ridge. Mendel & Sauter (1997) determined the location of seamounts along this portion of the SWIR and found that they are extremely sparse away from the large volcanic centres A deep-tow sidescan survey found no evidence of recent volcanism in an 82 km-long section between 64°31′E and 65°20′E (Sauter *et al.* 2004) in an area which trends nearly orthogonal to the spreading direction with an effective spreading rate of 13.2–14 mm yr^{-1}. In contrast, the area immediately to the west of the Melville Transform is associated with elongated volcanic ridges and the sidescan survey found that segments in this area are covered with volcanic terrain, most of it relatively fresh (Sauter *et al.* 2002; Gomez *et al.* 2006). Mendel & Sauter (1997) report a much higher and more evenly distributed population of seamounts in this region than to the east of the transform. This area, which appears similar to the WVZ on the Gakkel Ridge, has a trend of about N50°E and is thus about 40° from perpendicular to the spreading direction with an effective spreading rate of ∼10.7 mm yr^{-1}.

Thus, at the eastern SWIR, segments with an effective spreading rate <11 mm yr^{-1} have a more vigorous 'slow' or WVZ-like morphology and segments with an effective spreading rate >13 mm yr^{-1} have an amagmatic EVZ- or SMZ-like ultraslow morphology. Clearly, effective spreading rate is not the dominant factor controlling the form of axial tectonics at this area. As was the case for the transition from 'slow' to 'superslow' spreading at 3°E on the Gakkel Ridge, the Melville transform, separating these two areas on the SWIR is the location of a significant discontinuity in mantle composition (Meyzen *et al.* 2003, 2005).

CONCLUSIONS

A quantitative characterization of seamount volcanism along the axis of the Gakkel Ridge shows both that volcanism at the Gakkel Ridge is much reduced compared with the MAR and that there

are significant variations in the extent and distribution of volcanic features in different sections of the Gakkel Ridge. The density of constructional volcanic structures in the WVZ is 55% of that determined using the same techniques at the MAR and the characteristic height and the volume of seamounts at the WVZ axis is significantly less than at the MAR. These results imply a greatly reduced melt supply to the WVZ. These results are consistent with seismic results that suggest that the crustal thickness at the WVZ is approximately half that normally found at the MAR (Jokat & Schmidt-Aursch 2007). However, in spite of the severely reduced melt supply, the WVZ still demonstrates the basic pattern of MAR morphology with axial volcanic ridges, volcanoes scattered across the rift valley floor, and rift valley walls consisting of sets of high-angle faults. It thus appears that the 'slow spreading' form of crustal accretion characterized by partial focusing of melt to the centre of segments, redistribution of magma along-axis by dykes, and high-angle normal faulting (e.g. Smith & Cann 1993; Cannat 1996; Hooft *et al.* 2000; Magde *et al.* 2000; Dunn *et al.* 2005) can be maintained at the greatly reduced melt supply of the WVZ.

The Eastern Volcanic Zone displays a completely different mode of crustal accretion. The density of volcanic features is about 45% of that found at the WVZ (and about 25% of the density at the MAR). Seamounts cluster near the large magmatic centres but are observed along the entire length of the EVZ. Away from the magmatic centres, seamounts tend to be located at the edge of the rift valley or on the valley walls. The Sparsely Magmatic Zone displays the same pattern of volcanism as the WVZ but taken to an extreme. There are no seamounts on the valley floor for 185 km to the west and 45 km to the east of the 19°E volcanic centre. It appears that melt produced by melting of mantle upwelling in response to plate separation in the EVZ and SMZ is efficiently focused to widely spaced magmatic centres. Magma erupted between the magmatic centres reaches the surface along deep-cutting faults with the result that seamounts are occasionally found on the valley walls but rarely on the valley floor.

The transition between the two forms of crustal accretion is a threshold step between the two completely different modes that appears to occur when the cold lithospheric lid reaches a critical thickness. Spreading rate is one of several factors that affect which style of seafloor spreading occurs. On the Gakkel Ridge, the transition from the WVZ to the SMZ is localized by a major compositional boundary in the mantle (Goldstein *et al.* 2008).

ACKNOWLEDGMENTS

I thank Mark Behn for providing his seamount location algorithm and for assistance in implementing it, Margo Edwards of the University of Hawaii and Hans-Werner Schenke of the Alfred Wegner Institute played critical roles in the processing of the bathymetry data sets used in this study. D. K. Smith and W. Jokat provided thorough and thoughtful reviews that greatly improved the manuscript. The GMT software package (Wessel & Smith 1998) was used extensively for data analysis and the preparation of figures. This work was funded by NSF grant OPP-0352642. LDEO contribution 7167.

REFERENCES

Anderson, R.N., Spariosu, D.J., Weissel, J.K. & Hayes, D.E., 1980. The interrelationship between variations in magnetic anomaly amplitudes and basalt magnetization and chemistry along the Southeast Indian Ridge, *J. geophys. Res.,* **85,** 3883–3898.

Baker, E.T. *et al.*, 2004. Hydrothermal venting in magma deserts: the ultraslow-spreading Gakkel and Southwest Indian Ridges, *Geochem. Geophys. Geosyst.,* **5,** Q08002, doi:10.1029/2004GC000712.

Batiza, R., Fox, P.J., Vort, P.R., Cande, S.C., Grindlay, N.R., Melson, W.G. & O'Hearn, T., 1989. Morphology, abundance and chemistry of near-ridge seamounts in the vicinity of the Mid-Atlantic Ridge ∼26°S, *J. Geol.,* **97,** 209–220.

Behn, M.D., Sinton, J.M. & Detrick, R.S., 2004. Effect of the Galapagos hotspot on seafloor volcanism along the Galapagos Spreading Center (90.9–97.6°W), *Earth planet. Sci. Lett.,* **217,** 331–347.

Blackman, D.K., Cann, J.R., Janssen, B. & Smith, D.K., 1998. Origin of extensional core complexes: evidence from the Mid-Atlantic Ridge at Atlantis Fracture Zone, *J. geophys. Res.,* **103,** 21315–21333.

Bosworth, W., Huchon, P. & McClay, K., 2005. The Red Sea and Gulf of Aden Basins, *J. Afric. Earth Sci.,* **43,** 354–378.

Bown, J.W. & White, R.S., 1994. Variation with spreading rate of oceanic crustal thickness and geochemistry, *Earth planet. Sci. Lett.,* **121,** 435–449.

Brozena, J.M., Childers, V.A., Lawver, L.A., Gahagan, L.M., Forsberg, R., Faleide, J.I. & Eldholm, O., 2003. New aeromagnetic study of the Eurasia Basin and Lomonosov Ridge: implications for basin development, *Geology,* **31,** 825–828.

Buck, W.R., Lavier, L.L. & Poliakov, A.N.B., 2005. Modes of faulting at mid-ocean ridges, *Nature,* **434,** 719–723.

Cann, J.R. *et al.*, 1997. Corrugated slip surfaces formed at ridge transform intersections on the Mid-Atlantic Ridge, *Nature,* **385,** 329–332.

Cannat, M., 1996. How thick is the magmatic crust at slow spreading oceanic ridges?, *J. geophys. Res.,* **101,** 2847–2857.

Cannat, M., Rommevaux-Jestin, C. & Fujimoto, H., 2003. Melt supply variations to a magma-poor ultra-slow spreading ridge (Southwest Indian Ridge 61° to 69°E), *Geochem. Geophys. Geosyst.,* **4,** 9014, doi:10.1029/2002GC000840.

Cannat, M., Sauter, D., Mendel, V., Ruellan, E., Okino, K., Escartin, J., Combrier, V. & Baala, M., 2006. Modes of seafloor generation at a melt-poor ultraslow-spreading ridge, *Geology,* **34,** 605–608.

Chayes, D.N. *et al.*, 1996. SCAMP: an enhanced geophysical mapping system for Arctic submarine cruises, *EOS, Trans. Am. geophys. Un.,* **77,** F315.

Chayes, D.N. *et al.*, 1997. SCAMP: a submarine-mounted geophysical survey system for use under the the Artic ice, *in Proceedings of Oceans '97, IEEE, Halifax, NS*.

Chayes, D.N., Anderson, R.M., Ardai, J.L., Coakley, B.J., Davis, R.B., Edwards, M.H. & Rognstad, M.R., 1999. SCAMP Performance, *EOS, Trans. Am. geophys. Un.,* **80,** F1001.

Chu, D. & Gordon, R.G., 1999. Evidence for motion beqween Nubia and Somalia along the Southwest Indian Ridge, *Nature,* **398,** 64–67.

Coakley, B.J. & Cochran, J.R., 1998. Gravity Evidence of very thin crust at the Gakkel Ridge (Arctic Ocean), *Earth planet. Sci. Lett.,* **162,** 81–95.

Cochran, J.R., 2005. Northern Red Sea: nucleation of an oceanic spreading center within a continental rift, *Geochem. Geophys. Geosyst.,* **6,** Q03006, doi:10.1029/2004GC000826.

Cochran, J.R., Kurras, G.J., Edwards, M.H. & Coakley, B.J., 2003. The Gakkel Ridge: bathymetry, gravity anomalies and crustal accretion at extremely slow spreading rates, *J. geophys. Res.,* **108,** 2116, doi:10.1029/2002JB001830.

DeMets, C., Gordon, R.G., Argus, D.F. & Stein, S., 1994. Effect of recent revisions to the geomagnetic reversal time scale on estimates of current plate motions, *Geophys. Res. Lett.,* **21,** 2191–2194.

Detrick, R.S., Needham, H.D. & Renard, V., 1995. Gravity anomalies and crustal thickness variations along the Mid-Atlantic Ridge between 33°N and 40°N, *J. geophys. Res.,* **100,** 3767–3787.

Dick, H.J.B., Lin, J. & Schouten, H., 2003. An ultraslow-spreading class of ocean ridge, *Nature,* **426,** 405–412.

Dunn, R.A., Lekic, V., Detrick, R.S. & Toomey, D.R., 2005. Three-dimensional seismic structure of the Mid-Atlantic Ridge (35°N): evidence for focused melt supply and lower crustal dike injection, *J. geophys. Res.,* **110,** B09101, doi:10.1029/2004/JB003473.

Dupre, B. & Allegre, C.J., 1983. Pb-Sr isotope variation in Indian Ocean basalts and mixing phenomena, *Nature,* **303,** 142–146.

Edmonds, H.N. *et al.*, 2003. Discovery of abundant hydrothermal venting on the ultraslow-spreading Gakkel ridge in the Arctic Ocean, *Nature,* **421,** 252–256.

Edwards, M.H., Kurras, G.J., Tolstoy, M., Bohnenstiehl, D.R., Coakley, B.J. & Cochran, J.R., 2001. Evidence of recent volcanic activity on the ultraslow-spreading Gakkel Ridge, *Nature,* **409,** 808–812.

Forsyth, D.W., Ehrenbard, R.L. & Chapin, S., 1987. Anomalous upper mantle beneath the Australian-Antarctic Discordance, *Earth planet. Sci. Lett.,* **84,** 471–478.

Glebovsky, V.Y., Kovacs, L.C., Maschenkov, S.P. & Brozena, J.M., 2000. Joint compilation of Russian and US Navy aeromagnetic data in the central Arctic seas, *Polarforschung,* **68,** 35–40.

Glebovsky, V.Y., Kaminsky, V.D., Minakov, A.N., Merkurev, S.A., Childers, V.A. & Brozena, J.M., 2006. Formation of the Eurasian Basin in the Arctic Ocean as inferred from geohistorical analysis of the anomalous magnetic field, *Geotectonics,* **40,** 263–281.

Goldstein, S.L., Soffer, G., Langmuir, C.H., Lehnert, K., Graham, D.W. & Michael, P.J., 2008. Origin of a "Southern Hemisphere" geochemical signal in the Arctic upper mantle, *Nature,* **453,** 89–94.

Gomez, O., Briais, A., Sauter, D. & Mendel, V., 2006. Tectonics at the axis of the very slow spreading Southwest Indian Ridge: insights from TOBI side-scan sonar imagery, *Geochem. Geophys. Geosyst.,* **7,** Q05K12, doi:10.1029/2005GC000955.

Hart, S.R., 1984. A large-scale isotope anomaly in the Southern Hemisphere mantle, *Nature,* **309,** 753–757.

Hellebrand, E. & Snow, J.E., 2003. Deep melting and sodic metasonatism underneath the highly oblique-spreading Lena Trough (Arctic Ocean), *Earth planet. Sci. Lett.,* **216,** 283–299.

Hooft, E.E.E., Detrick, R.S., Toomey, D.R., Collins, J.A. & Lin, J., 2000. Crustal thickness and structure along three contrasting spreading segments of the Mid-Atlantic Ridge, 33.5°E-35°E, *J. geophys. Res.,* **105,** 8205–8226.

Hussenoeder, S.A., Kent, G.M. & Detrick, R.S., 2002. Upper crustal seismic structure of the slow spreading Mid-Atlantic Ridge, 35°N: constraints on volcanic emplacement processes, *J. geophys. Res.,* **107,** doi:10.1029/2001JB001691.

Jokat, W. & Schmidt-Aursch, M.C., 2007. Geophysical characteristics of the ultraslow spreading Gakkel Ridge, Arctic Ocean, *Geophys. J. Int.,* **168,** 983–998.

Jokat, W., Ritzmann, O., Schmidt-Aursch, M.C., Drachov, S., Gauger, S. & Snow, J.E., 2003. Geophysical evidence for reduced melt production on the Arctic ultraslow Gakkel mid-ocean ridge, *Nature,* **423,** 962–965.

Jordan, T.H., Menard, H.W. & Smith, D.K., 1983. Density and size distribution of seamounts in the Eastern Pacific inferred from wide-beam sounding data, *J. geophys. Res.,* **88,** 10508–10518.

Karasik, A.M., 1968. Magnetic anomalies of the Gakkel Ridge and origin of the Eurasia subbasin of the Arctic Ocean (in Russian), *Geofiz. Metody rezvedki v Arkite (Geophys. Methods of Prospecting in the Arctic),* **5,** 8–19.

Klein, E.M., Langmuir, C.H., Zindler, A., Staudigal, H. & Hamelin, B., 1988. Isotopic evidence of a mantle convecting boundary at the Australian-Antarctic discordance, *Nature,* **333,** 623–629.

Klein, E.M., Langmuir, C.H. & Staudigel, H., 1991. Geochemistry of basalts from the Southeast Indian Ridge, 115°E-138°E, *J. geophys. Res.,* **96,** 2089–2108.

Klingelhofer, F., Geli, L., Matias, L., Steinsland, N. & Mohr, J., 2000. Crustal structure of a super-slow spreading centre: a seismic refraction study of Mohns Ridge, 72°N, *Geophys. J. Int.,* **141,** 509–526.

Kuo, B.Y., 1993. Thermal anomalies beneath the Australian-Antarctic Discordance, *Earth planet. Sci. Lett.,* **119,** 349–364.

Lin, J., Purdy, G.M., Schouten, H., Sempere, J.C. & Zervas, C., 1990. Evidence from gravity data for focused magmatic accretion along the Mid-Atlantic Ridge, *Nature,* **344,** 627–632.

Macdonald, K.C., 1986. The crest of the Mid-Atlantic Ridge: models for crustal generation processes and tectonics, in *The Western North Atlantic Region,* pp. 51–68, eds Vogt, P. & Tucholke, B., Geological Society of America, Boulder, CO.

Magde, L.S., Barclay, A.H., Toomey, D.R., Detrick, R.S. & Collins, J.A., 2000. Crustal magma plumbing within a segment of the Mid-Atlantic Ridge, 35°N, *Earth planet. Sci. Lett.,* **175,** 55–67.

Mendel, V. & Sauter, D., 1997. Seamount volcanism at the super slow spreading Southwest Indian Ridge between 57°E and 70°E, *Geology,* **25,** 99–102.

Mendel, V., Sauter, D., Rommevaux-Jestin, C., Patriat, P., Lefebvre, F. & Parson, L.M., 2003. Magmato-tectonic cyclicity at the ultra-slow spreading Southwest Indian Ridge: evidence from variations of axial volcanic ridge morphology and abyssal hills pattern, *Geochem. Geophys. Geosyst.,* **4,** 9102, doi:10.1029/2002GC000417.

Meyzen, C.M., Toplis, M.J., Humler, E., Ludden, J.N. & Mevel, C., 2003. A discontinuity in mantle composition beneath the Southwest Indian Ridge, *Nature,* **421,** 731–733.

Meyzen, C.M., Ludden, J.N., Humler, E., Luais, B., Toplis, M.J., Mevel, C. & Storey, M., 2005. New insights into the origin and distributionof the DUPAL isotope anomaly in the Indian Ocean mantle from MORB of the Southeast Indian Ridge, *Geochem. Geophys. Geosyst.,* **6,** Q11K11, doi:10.1029/2005GC000979.

Michael, P.J. *et al.*, 2003. Magmatic and amagmatic seafloor generation at the ultraslow-spreading Gakkel Ridge, Arctic Ocean, *Nature,* **423,** 956–961.

Minshull, T.A., Muller, M.R. & White, R.S., 2006. Crustal structure of the Southwest indian Ridge at 66°E: seismic constraints, *Geophys. J. Int.,* **166,** 135–147.

Needham, H.D. & Francheteau, J., 1974. Some characteristics of the rift valley in the Atlantic Ocean near 36°48′ North, *Earth planet. Sci. Lett.,* **22,** 29–43.

Palmer, J., Sempere, J.C., Christie, D.M. & Phipps Morgan, J., 1993. Morphology and tectonics of the Australian-Antarctic Discordance between 123°E and 128°E, *Mar. geophys. Res.,* **15,** 121–152.

Patriat, P., 1987. Reconstitution de l'evolution du systeme de dorsales de l'ocean Indien par les methodes de la Cinematique des Plaques, *Territore des Terres Austales et Antarctiques, Fracaises, Paris,* 310p.

Patriat, P. & Segoufin, J., 1988. Reconstruction of the Central Indian Ocean, *Tectonophysics,* **155,** 211–234.

Pyle, D.G., Christie, D.M. & Mahoney, J.J., 1992. Resolving an isotopic boundary within the Australian-Antarctic Discordance, *Earth planet. Sci. Lett.,* **112,** 161–178.

Reid, I. & Jackson, H.R., 1981. Oceanic spreading rate and crustal thickness, *Mar. geophys. Res.,* **5,** 165–172.

Sauter, D., Patriat, P., Rommevaux-Jestin, C., Cannat, M., Briais, A. & Gellieni Shipboard Party, 2001. The Southwest Indian Ridge between 49°15′E and 57°E: focused accretion and magma redistribution, *Earth planet. Sci. Lett,,* **192,** 303–317.

Sauter, D., Parson, L.M., Mendel, V., Rommevaux-Jestin, C., Gomez, O., Briais, A., Mevel, C. & Tamaki, K., 2002. TOBI sidescan sonar imagery of the very slow spreading southwest Indian Ridge: evidence for along-axis magma distribution, *Earth planet. Sci. Lett,,* **199,** 81–95.

Sauter, D., Mendel, V., Rommevaux-Jestin, C., Parson, L.M., Fujimoto, H., Mevel, C., Cannat, M. & Tamaki, K., 2004. Focused magmatism versus amagmatic spreading along the ultra-slow spreading southwest Indian Ridge: evidence from TOBI side scan sonar imagery, *Geochem. Geophys. Geosyst.,* **5,** Q10K09, doi:10.1029/2004GC000738.

Sekretov, S.B., 1998. Southeastern Eurasian Basin termination: structure and key episodes of tectonic history, in *Proceedings of ICAM (International Conference on Arctic Margins) III (Abstracts)*, 165, Bundesanstalt f. Geow. & Rohstoffe, Hanover.

Sekretov, S.B., 2002. Structure and tectonic evolution of the southern Eurasian Basin, Arctic Ocean, *Tectonophysics,* **351,** 193–243.

Sempere, J.C., Purdy, G.M. & Schouten, H., 1990. Segmentation of the Mid-Atlantic Ridge between 24°N and 30°40′N, *Nature,* **344,** 427–431.

Sempere, J.C., Lin, J., Brown, H.S., Schouten, H. & Purdy, G.M., 1993. Segmentation and morphologic variations along a slow-spreading center: the Mid-Atlantic Ridge (24°00′N-30°40′N), *Mar. geophys. Res.,* **15,** 153–200.

Smith, D.K. & Cann, J.R., 1990. Hundreds of small volcanoes on the median valley floor of the Mid-Atlantic Ridge at 24–30°N, *Nature,* **348,** 152–155.

Smith, D.K. & Cann, J.R., 1992. The role of seamount volcanism in crustal construction at the Mid-Atlantic Ridge (24°-30°N), *J. geophys. Res.,* **97,** 1645–1658.

Smith, D.K. & Cann, J.R., 1993. Building the crust at the Mid-Atlantic Ridge, *Nature,* **365,** 707–715.

Smith, D.K. & Cann, J.R., 1999. Constructing the upper crust of the Mid-Atlantic Ridge: a reinterpretation based on the Puna Ridge, Kilauea Volcano, *J. geophys. Res.,* **104,** 25379–25399.

Smith, D.K. & Jordan, T.H., 1988. Seamount statistics in the Pacific Ocean, *J. geophys. Res.,* **93,** 2899–2918.

Smith, W.H.F. & Sandwell, D.T., 1997. Global sea floor topography from satellite altimetry and ship depth soundings, *Science,* **277,** 1956–1962.

Snow, J.E., Hellebrand, E., Jokat, W. & Muhe, R., 2001. Magmatic and hydrothermal activity in Lena Trough, Arctic Ocean, *EOS, Trans. Am. geophys. Un.,* **82,** 193,197–198.

Thiede, J., 2002. Polarstern Arktis XVII/2 Cruise Report: AMORE 2001, *Berichte zur Polar- und Meersforshung,* **421,** 1–397.

Tolstoy, M., Harding, A.J., Orcutt, J.A. & Phipps Morgan, J., 1995. Crustal thickness at the Australian Antarctic Discordance and neighboring Southeast Indian Ridge, *EOS, Trans. Am. geophys. Un.,* **76,** F570.

Tucholke, B.E., Lin, J. & Kleinrock, M.C., 1998. Magamullions and mullion structure defining metamorphic core complexes on the Mid-Atlantic Ridge, *J. geophys Res.,* **103,** 9857–9866.

Vogt, P.R., Taylor, P.T., Kovacs, L.C. & Johnson, G.L., 1979. Detailed aeromagnetic investigation of the Arctic Basin, *J. geophys. Res.,* **84,** 1071–1089.

Wang, X. & Cochran, J.R., 1993. Gravity anomalies, isostasy and mantle flow at the East Pacific Rise crest, *J. geophys. Res.,* **98,** 19 505–19 531.

Wang, X. & Cochran, J.R., 1995. Along-axis gravity gradients at mid-ocean ridges: implications for mantle flow and axis morphology, *Geology,* **23,** 29–32.

Weissel, J.K. & Hayes, D.E., 1974. The Australian Antarctic Discordance: new results and implications, *J. geophys. Res.,* **79,** 2579–2587.

Wessel, P. & Smith, W.H.F., 1998. New improved version of Generic Mapping Tools released, *EOS, Trans. Am. geophys. Un.,* **79,** 579.

West, B.P., Sempere, J.-C., Pyle, D.G., Phipps Morgan, J. & Christie, D.M., 1994. Evidence for variable upper mantle temperature and crustal thickness in and near the Australian-Antarctic Discordance, *Earth planet. Sci. Lett.,* **128,** 135–153.

White, R.S., McKenzie, D. & O'Nions, R.K., 1992. Oceanic crustal thickness from seismic measurements and rare earth element inversions, *J. geophys. Res.,* **97,** 19683–19 715.

White, S.M., Macdonald, K.C., Scheirer, D.S. & Cormier, M.H., 1998. Distribution of isolated volcanoes on the flanks of the East Pacific Rise, 15.3°S-20°S, *J. geophys. Res.,* **103,** 30371–30384.